STATIONARY PERIODIC PATTERNS IN THE 1D GRAY-SCOTT MODEL*

DAVID S. MORGAN†, ARJEN DOELMAN‡, AND TASSO J. KAPER§

Abstract. In this work, we study the existence and stability of a family of stationary periodic patterns in the 1D Gray-Scott model. First, it is shown that these periodic solutions are born at a critical parameter value in a Turing/Ginzburg-Landau bifurcation, and an analysis of the appropriate Ginzburg-Landau normal form equation reveals that they exist below the critical parameter. Next, we analytically continue this family of periodic solutions in the ordinary differential equation for stationary solutions from the regime in which they are born and in which their spatial periods are $\mathcal{O}(1)$, to the regime where their spatial periods are asymptotically large. Depending on parameter values, the family terminates in global bifurcations via homoclinic orbits or in local bifurcations.

In addition to establishing these existence results, we perform a stability analysis. For parameter values near the critical parameter, there is an Eckhaus subband of stable periodic states within each existence interval. Moreover, these subbands of stable periodic states are continued into the full parameter range in which existence is shown. This numerical continuation is carried out all the way down into the regime where the periods of the orbits are asymptotically large and for which we have recently published analytical stability results. Taken together, these stability results show that there is a Busse balloon of stable stationary periodic solutions in the parameter space.

Finally, in numerical simulations, these stable periodic states are observed to be attractors for a wide variety of initial data, including data consisting of large-amplitude fronts moving into intervals over which the concentrations are in a linearly stable homogeneous state, data consisting of small-amplitude (Swift-Hohenberg like) fronts moving into intervals on which the concentrations are in a linearly unstable homogeneous state, and general oscillatory data.

1. Introduction. The Gray-Scott model [16, 17], governing chemical reactions of the form $\mathcal{U} + 2\mathcal{V} \to 3\mathcal{V}$ and $\mathcal{V} \to \mathcal{P}$, consists of the following coupled pair of reaction-diffusion equations:

$$\frac{\partial U}{\partial t} = D_U \Delta U - UV^2 + A(1 - U)$$

(1.1)

$$\frac{\partial V}{\partial t} = D_V \Delta V + UV^2 - BV.$$

Here A and B are rate constants, D_U and D_V are the diffusivities, $U \equiv U(x, t)$ and $V \equiv V(x, t)$ are the concentrations of the chemical species $\mathcal{U}$ (the inhibitor) and $\mathcal{V}$ (the activator), and Δ is the Laplacian operator.

It has recently been discovered numerically and experimentally that the Gray-Scott model exhibits a wide variety of spatial and time-dependent patterns [27, 24, 23]. These works report on the evolution of circular spots in two dimensions. The spots, in which the concentration of $\mathcal{V}$ is high and that of $\mathcal{U}$ is low, were observed to undergo a self-replication process in which an initial spot evolved into multiple spots, with the time asymptotic state depending on the system parameters, or, for example, the

---

interior of the spot collapsed, leaving behind an annular ring of high $\mathcal{V}$ and low $\mathcal{U}$ concentrations.

Self-replication was also observed and analyzed in 1D simulations, see [29, 28, 30, 6, 7, 26, 8, 4, 25]. In 1D, the regions of high $\mathcal{V}$ and low $\mathcal{U}$ concentrations are intervals, so that the $\mathcal{V}$ concentration profile exhibits a pulse in the interval. Depending on the system parameters, these pulses can be stationary or they can split into two pulses which, after the splitting event, move apart from each other and split again. A full stability analysis of the stationary, single-pulse homoclinic states and the stationary spatially-periodic states with large spatial periods is contained in [7, 8] for a certain family of scalings, and an existence and stability analysis of slowly-modulated pulse solutions whose small wave speeds decrease slowly in time is given in [4] for general scalings. It was also shown in [6, 7] that stationary, spatially-periodic solutions with asymptotically large spatial periods are attractors in the self-replication regime. Finally, in [7], two sequences of bifurcation curves are identified. In the first, these periodic states with asymptotically large spatial periods undergo subcritical Hopf bifurcations and become stable solutions of (1.1). In the second sequence, the bifurcation curves correspond to the boundary of the existence domains (or 'disappearance values') of each of the periodic states as stationary solutions of (1.1), and these latter bifurcation values agree well with the numerically observed transition values in the splitting regime. For example, when the parameters are such that the two-pulse solution does not exist but 3- and higher-pulse solutions do exist, then two-pulse initial data is observed to split into a 3- or 4-pulse solution.

In other parameter regimes, the Gray-Scott model, as well as a related autocatalytic system, exhibits kink solutions, front solutions and heteroclinic traveling waves, see [1, 13, 18].

Motivated by the experiments and simulations of Pearson [27], attention is primarily focused on the case in which the diffusivity of the inhibitor $\mathcal{U}$ is greater than that of the activator $\mathcal{V}$. In this case, $\mathcal{U}$ is able to rapidly reach the localized regions of high $\mathcal{V}$ concentration and hence sustain the reaction, while the relatively slow diffusion of $\mathcal{V}$ makes it possible for these localized regions to persist. We thus set $D_u = 1$ and introduce the small parameter δ by setting $D_V = \delta^{2\sigma}$, with $0 < \delta \ll 1$ and $\sigma \geq 0$. This choice of the diffusion coefficient D_V will enable us to explore a wide region of parameter space.

Depending on the values of A and B, there are either one or three homogeneous stationary states. One such state, $U \equiv 1$, $V \equiv 0$, exists and is linearly stable for all $A, B > 0$. In addition, when $4B^2 < A$, there are two other stationary states at

$$(1.2) \qquad (U_{\pm}, V_{\pm}) = \left(\frac{1}{2}\left[1 \pm \sqrt{1 - \frac{4B^2}{A}} \right], \frac{A}{2B}\left[1 \mp \sqrt{1 - \frac{4B^2}{A}} \right] \right).$$

The nullclines of the reaction o.d.e.:

$$\dot{U} = -UV^2 + A(1 - U) \quad \text{and} \quad \dot{V} = UV^2 - BV.$$

are illustrated in Figure 1.1. The U nullcline is given by the graph of $\pm\sqrt{\frac{A}{U} - A}$. The V nullcline consists of the U-axis together with one branch of a hyperbola in the first quadrant, asymptoting onto the U and V axes. These nullclines intersect at $(1, 0)$ for all A and B. In addition, they have a point of tangency at $4B^2 = A$; and, for $4B^2 < A$, the two additional intersection points $(U_{\pm}, V_{\pm})$ exist. Thus, there is a saddle-node bifurcation when $4B^2 = A$. See Figures 1.1a-b.
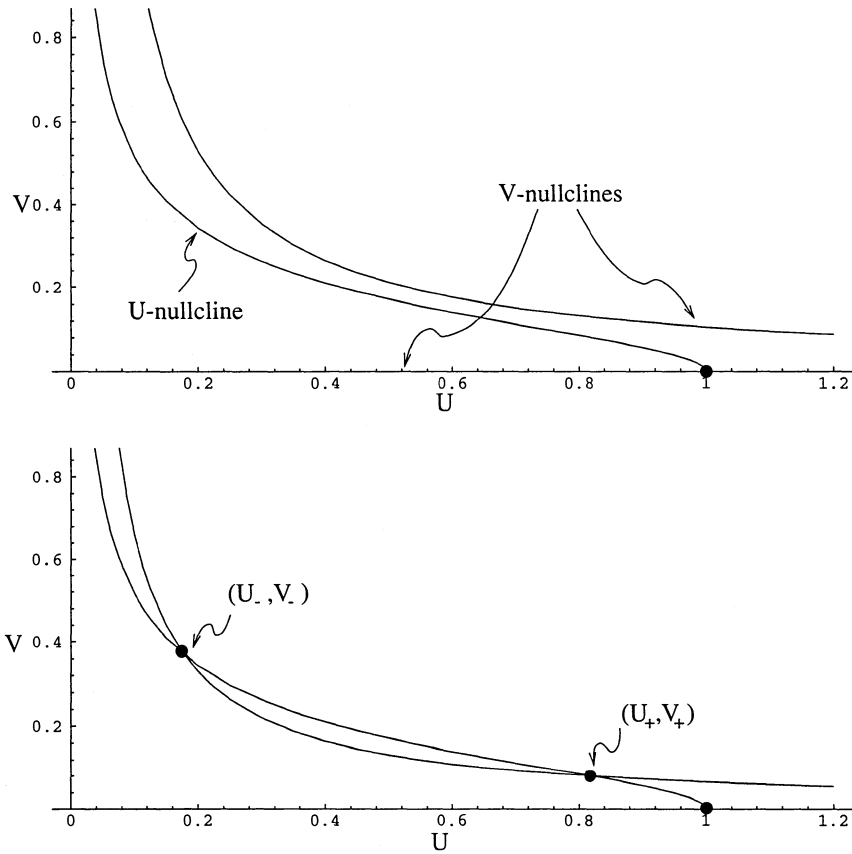
FIG. 1.1. **a.** *The plot of the nullclines for of the reaction terms when* $4B^2 > A$. **b.** *The plot of the nullclines of the reaction terms when* $4B^2 < A$.

In this work, we present an existence and stability analysis for a family of stationary, spatially-periodic states in the 1D Gray-Scott model, with $x \in \mathbb{R}$. Most of these periodic states exist in the regime where $4B^2 < A$, and they oscillate about the state (U_-, V_-). This family is born at a critical value A_c of the parameter A in a Turing/Ginzburg-Landau bifurcation (see Section 3 for a definition of this bifurcation). For each A less than and sufficiently close to A_c, we show that there exists a band of periodic states within some wave number interval, and the length of the spatial period is $\mathcal{O}(1)$ with respect to δ. Then, using results of Eckhaus [10] and Schneider [34], we show that within each of these existence bands there exists a subband of wave numbers for which the periodic states are nonlinearly stable.

Having established these existence and stability results for A less than, but sufficiently close to, A_c, we turn our attention to smaller values of A well below A_c. In this regime, we present a constructive existence proof for stationary, spatially-periodic states with successively larger spatial periods as A decreases, ranging from $\mathcal{O}(1)$ to asymptotically large periods that scale with inverse powers of δ. These states are the continuation of those just described for A near A_c. Moreover, those with the asymptotically large periods exist in the other domain where $4B^2 > A$, and they are singular in nature, because they consist of fast and slow segments. Their existence is

established using geometric singular perturbation theory and the adiabatic Melnikov function. In addition, we show that these singular periodic orbits limit on certain fast-slow homoclinic orbits, whose existence was established for a restricted choice of parameters in [6].

Finally, we continue the stability results out of the regime in which A is close to A_c to the entire range of smaller A values for which existence has been established. Through numerical simulations, we observe that the widths of the continuations of the Eckhaus subbands decrease to zero eventually as A decreases to a bifurcation value A_{Hopf}, and the period of the orbits grows toward infinity, which is the spatial 'period' of the homoclinic orbit. At $A = A_{\text{Hopf}}$, the homoclinic pulse loses its stability by a Hopf bifurcation, see [7, 8, 4]. This numerical continuation therefore brings us down into the domain in which the stability results of [7, 8, 4] are valid. In [7, 8], we have used matched asymptotic expansions and a stability index analysis to identify the regime in which the singular periodic orbits with asymptotically large spatial periods are stable, and in [4], we have extended the asymptotic analysis to a general scaling and to include slowly-modulating pulse solutions. Taken together, the stability results of the present work and those of [7, 8, 4] may be characterized as a Busse balloon (see [3]), and they form a complete, jointly analytical and numerical, picture of a rich family of stable periodic states.

The periodic orbits whose existence and stability we demonstrate here derive their importance from the fact that they are seen to be attractors for a wide variety of initial data. First, we used data consisting of a localized, large amplitude perturbation of the stable uniform stationary state $U \equiv 1$, $V \equiv 0$. A large amplitude perturbation 'kicks' this linearly stable stationary state into the basin of attraction of the periodic orbit. In particular, the periodic pattern is formed as the large amplitude pulse (in V) moves outward from the center of the pattern, depositing the periodic pattern behind it. Second, we examined the evolution of data consisting of a small amplitude perturbation of the (unstable) stationary state (U_-, V_-) and saw the formation of the same periodic orbit. A similar phenomena is also observed in the Swift-Hohenberg equation [13], where a front propagates into a linearly unstable medium and deposits a stationary, spatially-periodic solution behind it. This second case is an example of the method of pattern formation discussed by A. Turing in his 1952 paper [37]. Finally, we considered general oscillatory initial data with Neumann boundary conditions that also evolved into stationary, spatially periodic states. See Figures 1.2a-b.

The analysis presented here complements that of [6] in the following way. In Theorems 4.2 and 4.3 of [6], stationary, spatially-periodic solutions were found for a certain special family of parameter values and the concentration of $\mathcal{V}$ was exponentially small in the intervals between pulses for these solutions. In this paper we determine the full family of periodic solutions for general $A, B > 0$ and $D_V \leq \mathcal{O}(D_U)$: unlike in [6] we do not a priori impose conditions on the relative magnitudes of A, B and D, and unlike [6] we do not focus only on the singular solutions.

Nevertheless, the relative magnitudes of A, B and D do play an extremely important role in the analysis in this paper. This is made explicit by writing $A = a\delta^\alpha$ and $B = b\delta^\beta$ (where we assume that a and b are $\mathcal{O}(1)$ with respect to $\delta \ll 1$, see also (2.3)). For any given σ (recall that δ and $\sigma \leq 0$ were defined by $D_V = \delta^{2\sigma}$) there are 3 important lines in the (α, β)-parameter space: $\ell_{TGL} = \{\beta = \frac{2}{3}(\alpha + \sigma)\}$, $\ell_{SN} = \{\beta = \frac{1}{2}\alpha\}$ and $\ell_{hom} = \{\beta = \frac{1}{3}(\alpha - 2\sigma)\}$. Note that ℓ_{TGL} and ℓ_{hom} determine a 'wedge' in the (α, β)-plane with ℓ_{SN} inside and that the 3 lines intersect in one point.
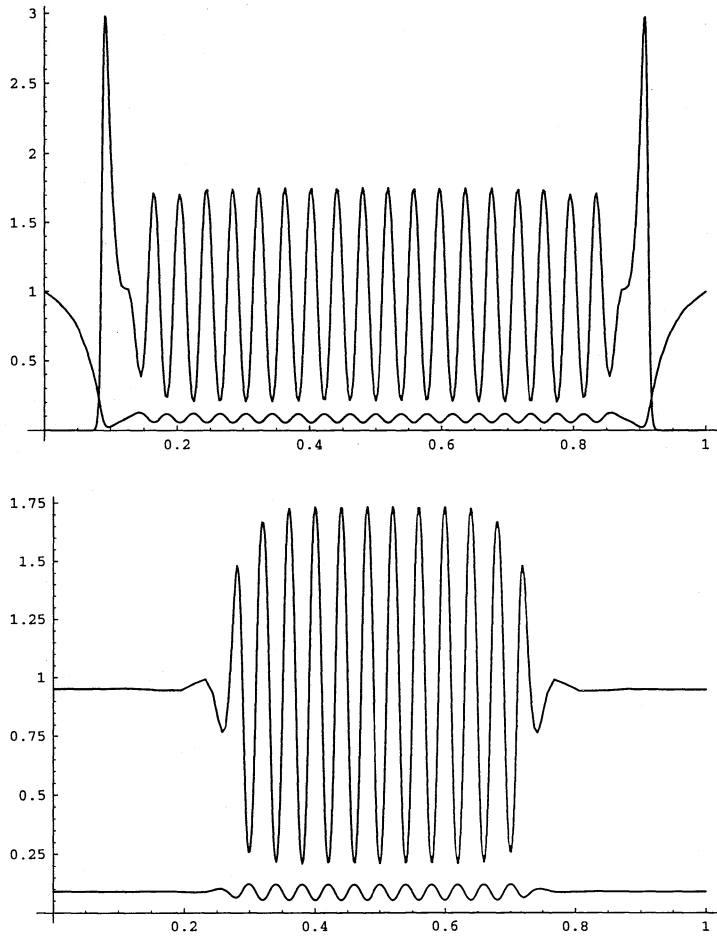
FIG. 1.2. **a.** *Simulation of (1.1) using 401 moving grid points for $A = 0.09$, $B = 0.086$, $D_u = 1$, $D_v = 0.01$ and $T_e = 1000$, with initial data given by $U = 1 - 0.5\sin^{100}(\pi x)$, $V = 0.25\sin^{100}(\pi x)$. The boundary conditions were of Dirichlet type, with $U(0,t) = U(1,t) = 1$ and $V(0,t) = V(1,t) = 0$.* **b.** *Simulation of (1.1) in which the same parameters were used as in frame a, with the exception that $T_e = 750$. The initial data used in this case was $U = U_- + 0.1\sin^{100}(\pi x)$, $V = V_- - 0.1\sin^{100}(\pi x)$, and the boundary conditions, though again of Dirichlet type, were $U(0,t) = U(1,t) = U_-$ and $V(0,t) = V(1,t) = V_-$. In both cases there is a dynamic process going on that is creating a spatially periodic stationary pattern. In a., large amplitude fronts propagate into intervals in which the system is in a linearly stable homogeneous state; and in b., a pair of small-amplitude fronts into a regime in which the system is in a linearly unstable homogeneous state (the classical Turing instability). In both simulations, the fronts 'deposit' a spatially periodic stationary core behind themselves.*

We show in section 3 that there is a family of periodic patterns that is created by a so-called 'Turing/Ginzburg-Landau' bifurcation as (α, β) decreases through the line ℓ_{TGL}. We follow this family of periodic patterns analytically through the wedge region and find (in section 5) that it 'disappears' by a saddle node bifurcation of homoclinic orbits as (α, β) decreases through ℓ_{hom}. The line ℓ_{SN} separates the wedge between ℓ_{TGL} and ℓ_{hom} into a region with (mostly) regular periodic patterns (sections 3 and 4) and a region with only singular periodic patterns of the structure studied in [6] (section 5).

In Section 2, we develop the relevant scaled equations. In Section 3, we establish the existence and stability of periodic states for $|A - A_c| \ll \mathcal{O}(1)$. The existence proof for general A below A_c is given in Section 4. We show analytically in Section 5 how these periodic orbits can be continued into the regime in parameter space where the fixed point (U_-, V_-) no longer exists. In Section 6 we compare our analysis to the results of numerical simulations, and we extend the stability results of Section 3 by numerically finding the edges of a Busse balloon. There are also two appendices containing the outlines of some necessary technical calculations.

2. Preliminary analysis of the system governing stationary spatial patterns.
Stationary patterns of (1.1) are solutions $(u(x), p(x), v(x), q(x))$ of the following system of ordinary differential equations:

$$
\begin{aligned}
u' &= p \\
p' &= uv^2 - A(1 - u) \\
\delta^\sigma v' &= q \\
\delta^\sigma q' &= -uv^2 + Bv,
\end{aligned}
$$

(2.1)

where $' \equiv \frac{d}{dx}$. It will be convenient for the analysis to consider a range of magnitudes of the feed and decay rates, and so we write them as: $A = \delta^\alpha a$ and $B = \delta^\beta b$, where $\alpha, \beta \geq 0$, as noted in the Introduction.

Using these scalings for A and B, we obtain the relevant leading order scalings for u and v, as follows. Since we will find that the periodic states are born in a Turing/Ginzburg-Landau bifurcation at the fixed point (U_-, V_-), it is useful to scale the variables u and v with the sizes of U_- and V_-, as expressed in terms of the scalings of A and B. To leading order, one has for $2\beta > \alpha$:

$$
(U_-, V_-) = \left(\delta^{2\beta - \alpha} \frac{b^2}{a}, \delta^{\alpha - \beta} \frac{a}{b} \right).
$$

(2.2)

Therefore, we set $u = \delta^{2\beta - \alpha} \hat{u}$ and $v = \delta^{\alpha - \beta} \hat{v}$.

Substituting these scalings into (2.1), we derive scalings for the other variables as follows. For the v-q subsystem, there is a distinguished limit when the linear and nonlinear terms in the q component of the vector field are of the same order and when the right-hand sides of both equations evolve on the same time scale, which imply a natural scaling for q. The same is true for p in the u-p subsystem. Finally, we do a rescaling of the independent variable. The scalings are:

$$
\begin{aligned}
A &= \delta^\alpha a, \quad B = \delta^\beta b, \quad x = \delta^{\sigma - \frac{\beta}{2}} \hat{\eta} \\
u &= \delta^{2\beta - \alpha} \hat{u}, \quad p = \delta^\beta \hat{p}, \quad v = \delta^{\alpha - \beta} \hat{v}, \quad q = \delta^{\alpha - \frac{\beta}{2}} \hat{q}.
\end{aligned}
$$

(2.3)

Defining $\epsilon = \delta^{\sigma - \frac{3}{2}\beta + \alpha}$ and using $\dot{} \equiv \frac{d}{d\hat{\eta}}$, we obtain the scaled system

$$
\begin{aligned}
\dot{\hat{u}} &= \epsilon \hat{p} \\
\dot{\hat{p}} &= \epsilon [\hat{u}\hat{v}^2 - a(1 - \delta^{2\beta - \alpha} \hat{u})] \\
\dot{\hat{v}} &= \hat{q} \\
\dot{\hat{q}} &= -\hat{u}\hat{v}^2 + b\hat{v}.
\end{aligned}
$$

(2.4)

The term $\delta^{2\beta - \alpha}$ in (2.4) may be expressed in terms of ϵ, as follows. From the definition of ϵ, one sees that $\delta^{2\beta - \alpha} = \epsilon^\rho$, where

$$
\rho = \frac{2\beta - \alpha}{\sigma - (3/2)\beta + \alpha}.
$$

(2.5)

However, clearly this equation for ρ only makes sense when the denominator is not zero. Many of the results in this work (see Sections 4 and 5) will be for the regime $\beta < (2/3)(\sigma + \alpha)$, so that the denominator is positive. In the case of $\beta = (2/3)(\sigma + \alpha)$ when the denominator vanishes, which will also play an important role in this work (see Section 3), we will simply define $\epsilon^\rho = \delta^{2\beta - \alpha}$. Observe, therefore, that it is possible, as we will see shortly, to have $\epsilon = 1$ (*i.e.*, $\beta = (2/3)(\sigma + \alpha)$) and $\epsilon^\rho \ll 1$ (*i.e.*, $2\beta - \alpha > 0$) at the same time.

We shall see in Section 4 that the $\hat{v}$-$\hat{q}$ subsystem of the scaled system (2.4) has the requisite balance of terms to support nontrivial periodic orbits with $\mathcal{O}(1)$ periods. We drop hats in the remainder of this section and in Sections 4-6, unless stated otherwise. Also, in Section 5, see especially Remark 5.2, we state the explicit connection between this scaled system and the systems studied in [6, 7, 8].

An observation that will be central to the analysis of (2.4) is that it possesses the following symmetry:

$$(2.6) \qquad (u, p, v, q, \eta) \to (u, -p, v, -q, -\eta).$$

This symmetry will be used in proving the existence of periodic orbits, also of the singular periodic orbits in Section 5 for which further scaling is used.

In order for the evolution of the u-p subsystem to be slower than, and no faster than, that of the v-q subsystem, one requires $\beta \leq \frac{2}{3}(\sigma + \alpha)$. In addition, for most of the analysis in this work (*i.e.*, everywhere except in part of Theorem 4.3, Section 5, and parts of Section 6), we work in the regime $4B^2 < A$ for vanishing δ, hence we require that $2\beta - \alpha \geq 0$, with $4b^2 < a$ in the case of equality. Summarizing, we have the following primary range for our parameters for the analysis in Sections 2-4:

$$(2.7) \qquad \beta \leq \frac{2}{3}(\sigma + \alpha) \quad \text{and} \quad 0 \leq 2\beta - \alpha.$$

In the scaled system (2.4), the fixed point $(u_-, 0, v_-, 0)$ is given to leading order by $(b^2/a, 0, a/b, 0)$. Thus, the linearization of (2.4) there is:

$$(2.8) \qquad \begin{pmatrix} \dot{u} \\ \dot{p} \\ \dot{v} \\ \dot{q} \end{pmatrix} = \begin{pmatrix} 0 & \epsilon & 0 & 0 \\ \epsilon \frac{a^2}{b^2} + \epsilon^{1+\rho} a & 0 & \epsilon 2b & 0 \\ 0 & 0 & 0 & 1 \\ -\frac{a^2}{b^2} & 0 & -b & 0 \end{pmatrix} \begin{pmatrix} u \\ p \\ v \\ q \end{pmatrix}.$$

The roots of the characteristic polynomial are of the form

$$(2.9) \quad (\lambda^2)_\pm = -w \pm \sqrt{w^2 - \epsilon^2 \left(\frac{a^2}{b} - \epsilon^\rho ab \right)}, \quad \text{where} \quad w = \frac{1}{2}(b - \epsilon^2 \frac{a^2}{b^2} - \epsilon^{2+\rho} a).$$

When $\rho > 0$, $(\lambda^2)_\pm < 0$ for vanishing ϵ, so that the fixed point $(u_-, 0, v_-, 0)$ is elliptic-elliptic. Then, when $\rho = 0$, the fixed point $(u_-, 0, v_-, 0)$ is also elliptic-elliptic as long as $b^2 < a$. Since $\rho = 0$ implies that $2\beta = \alpha$, the condition $4B^2 < A$ implies that $4b^2 < a$, and hence $b^2 < a$ and we see that this extra requirement is automatically satisfied.

The boundary of the domain in which the fixed point $(u_-, 0, v_-, 0)$ is elliptic-elliptic occurs when $\beta = \frac{2}{3}(\alpha + \sigma)$, where we encounter a reversible 1:1 resonant Hopf

bifurcation point (*i.e.*, two coincident pairs of purely imaginary eigenvalues). In this case, $\rho > 0$, $\epsilon = \delta^{\sigma - \frac{3}{2}\beta + \alpha} = 1$, and $\epsilon^\rho = \delta^{2\beta - \alpha} \ll 1$. We then have to leading order:

$$(2.10) \qquad (\lambda^2)_\pm = -w \pm \sqrt{w^2 - \frac{a^2}{b}}, \qquad \text{where} \qquad w = \frac{b}{2}\left(1 - \frac{a^2}{b^3}\right).$$

The expression under the square root is zero when

$$(2.11) \qquad a_c^2 = b^3(3 - 2\sqrt{2}).$$

Thus, because $w > 0$ and $a = a_c$, there are two coincident pairs of pure imaginary eigenvalues, and hence a reversible 1:1 resonance Hopf bifurcation, as indicated above. Moreover, beyond this bifurcation point, the two pairs of eigenvalues separate and move into the complex plane, gaining nontrivial real parts also. This bifurcation will be the starting point of the analysis in Section 3.

For completeness, we note that the expression for the square root in (2.10) is also zero when $a_c^2 = b^3(3 + 2\sqrt{2})$. For this root, however, we readily see that $w < 0$ and $(\lambda^2)_\pm > 0$, so that all four eigenvalues are real. Hence, the fixed point is of saddle-saddle type, and one does not expect to find periodic orbits lying nearby. Also, it is toward these points on the real-λ axis that the pairs of complex conjugate eigenvalues migrate, and afterwards they remain strictly real.

We conclude this section by examining the phase space of the scaled equation (2.4). When $\epsilon = 0$, the plane $\mathcal{M} = \{(u, p, v, q) | v, q = 0\}$ is trivially invariant, consisting of equilibria. Also, the v-q subsystem is a 1-parameter family of Hamiltonian systems with parameter u and Hamiltonian

$$(2.12) \qquad K = \frac{1}{2}q^2 + \frac{u}{3}v^3 - \frac{b}{2}v^2.$$

This system has a center equilibrium at $(v, q) = (\frac{b}{u}, 0)$ and a saddle equilibrium at the origin, see Figure 2.1. Note that when $u = b^2/a$, the center equilibrium corresponds to the leading order stationary state V_-.

For $0 < \epsilon \ll 1$, $\mathcal{M}$ is still invariant, and the flow on $\mathcal{M}$ is linear, with a saddle equilibrium at $(u, p) = (\epsilon^{-\rho}, 0)$. In particular, the flow on $\mathcal{M}$ is slow, and hence $\mathcal{M}$ is a slow manifold for the full system. See [12] for the theory of slow manifolds in singularly perturbed systems. The u-p subsystem on $\mathcal{M}$, may be examined using the independent variable $\psi = \epsilon\eta$:

$$(2.13) \qquad \begin{aligned} u' &= p \\ p' &= -a + \epsilon^\rho a u. \end{aligned}$$

The equilibrium has eigenvalues $\lambda_\pm = \pm\epsilon^{\rho/2}\sqrt{a}$ and associated eigenvectors

$$(2.14) \qquad (u, p)^T = (1, \pm\epsilon^{\rho/2}\sqrt{a})^T.$$

By linearity, the stable and unstable manifolds (lines) ℓ^s and ℓ^u of the saddle fixed point are given (see Figure 2.2) as the graph of:

$$p = \mp\epsilon^{\rho/2}\sqrt{a}(u - \epsilon^{-\rho}).$$

REMARK 2.1. There are three parameters: A, B, D_V, in the partial differential equation (1.1), where without loss of generality D_U is set to one. In the ordinary
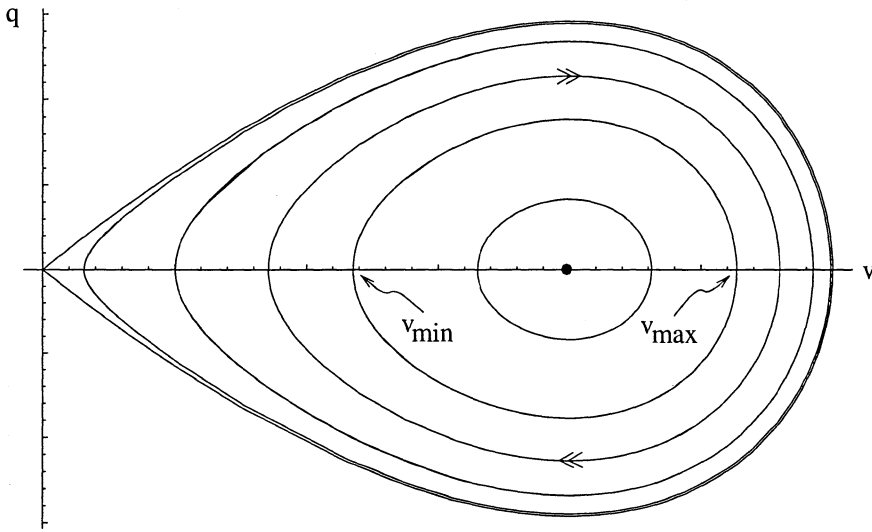
FIG. 2.1. *The phase plane of the fast subsystem, showing some periodic orbits and the orbit homoclinic to $(v = 0, q = 0)$.*

differential equations (2.4), there are five: α, β, σ, a, and b, where a and b are $\mathcal{O}(1)$ with respect to δ. The rescaling therefore introduces a redundancy in that stationary solutions of the partial differential equation which exist for a given triple of parameter values will be found for some set of triples of scaling exponents α, β, and σ (and the corresponding values of a and b) in the ordinary differential equations. It will be important to recall this fact at several points in the analysis, especially in subsection 3.1, where we analyze the Turing/Ginzburg-Landau bifurcation that occurs at a particular A_c (for each B) in the partial differential equation and that is recovered in the ordinary differential equations by using any triple of scaling exponents chosen from a set satisfying $\sigma = (3/2)\beta - \alpha$.

REMARK 2.2. In [6], [7], [8], the existence and stability of one-pulse and multipulse homoclinic solutions is studied when $\sigma = 1$, $\alpha = 2$ and $\beta \in [0,1)$, and in [7], $\beta = 1$ is also analyzed. In addition, in [4], we analyze the existence and stability of stationary and slowly-modulating homoclinic solutions for a much broader class of scalings.

REMARK 2.3. We will obtain some existence results for $\sigma < 0$ in Section 4. However, our stability results will not apply to this regime.

3. Bifurcating periodic solutions: $\beta = \frac{2}{3}(\sigma + \alpha)$. In this section, we study the behavior of the solutions of (1.1) near the reversible 1:1 resonance Hopf bifurcation point (2.11). The local normal form theory for reversible vector fields (see [20] and references therein) enables us to obtain a detailed description of the phase space of (2.4) in the neighborhood of such a critical point for parameters close to the bifurcation value. It can be shown by this normal form approach that there exists in (2.4), for any a close enough (and in our case below) a_c, a 1-parameter family of periodic solutions close to the fixed point $(u_-, 0, v_-, 0)$.
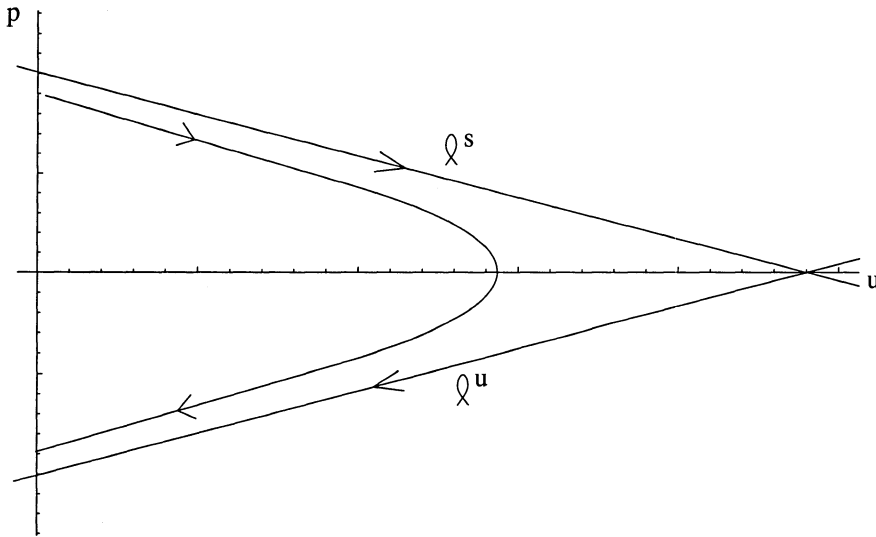
FIG. 2.2. *The phase plane of the linear slow subsystem on $\mathcal{M}$, showing the stable and unstable manifolds ℓ^s and ℓ^u of the saddle fixed point, as well as a branch of a hyperbola Γ_C inside these lines.*

The reversible 1:1 resonance Hopf bifurcation in the stationary problem associated to (1.1) is closely related to the bifurcation in the PDE at which the trivial pattern $(U = U_-, V = V_-)$ loses its stability, [19]. In this context, the elliptic-elliptic character (two noncoincident pairs of pure imaginary eigenvalues) of the critical point $(u_-, 0, v_-, 0)$ after the bifurcation (*i.e.*, for $A < A_c$) corresponds to the existence of a band of unstable wavenumbers centered around a critical wavenumber k_c (recall that 'time' in (2.4) is the spatial variable x of (1.1)). In hydrodynamic stability problems on unbounded domains, this bifurcation has been the main motivation to develop the concept of so-called modulation equations. The Ginzburg-Landau equation is the most well-known and generic example of such a modulation equation (see [9] for a review). The Ginzburg-Landau equation gives a weakly nonlinear description of the appearance of a band of stable spatially periodic solutions at near critical conditions. Turing studied the linear character of a similar bifurcation in the field of biological pattern formation [37]. The stationary patterns emerging from this bifurcation are called Turing patterns in reaction-diffusion equations. Therefore, we refer to this bifurcation as the 'Turing/Ginzburg-Landau bifurcation' in this paper.

In this section, we have chosen to approach this bifurcation along the lines of the theory of modulation equations since it gives clear insight into the behavior of the solutions of (1.1). In subsection 3.1, we study the linearized stability of the trivial pattern $(U = U_-, V = V_-)$ and recover the reversible 1:1 resonance Hopf bifurcation of Section 2. Then, in subsection 3.2, we formally derive a Ginzburg-Landau equation that describes the evolution of small perturbations of $(U = U_-, V = V_-)$ for parameter values close to the bifurcation. From this equation we obtain the existence of a 1-parameter family of stationary, spatially periodic solutions (with small amplitude) within which lies a subfamily of stable periodic solutions (the so-called Eckhaus band [10]). Finally, in subsection 3.3, the diffusive stability with respect to the PDE of

the solutions within the Eckhaus bands will be shown rigorously by appealing to the recent results of Schneider [34]. Note that throughout Section 3, we use capital letters U and V to denote the variables of the PDE (1.1).

3.1. Linear stability analysis of (U_-, V_-) and the determination of a_c.
We begin by linearizing (1.1) around the stationary state (U_-, V_-). Let

$$(3.1) \qquad (U, V) = (U_- + U(t)e^{ikx}, V_- + V(t)e^{ikx}),$$

where k is real and where we note that this Fourier decomposition is possible since we consider $x \in \mathbb{R}$. The linearization of (1.1) is:

$$(3.2) \qquad \begin{pmatrix} \dot{U} \\ \dot{V} \end{pmatrix} = \begin{pmatrix} -k^2 - V_-^2 - \delta^\alpha a & -2\delta^\beta b \\ V_-^2 & -\delta^{2\sigma}k^2 + \delta^\beta b \end{pmatrix} \begin{pmatrix} U \\ V \end{pmatrix},$$

where we have used $U_- V_- = \delta^\beta b$. We label the matrix M.

Using the trace-determinant representation of the eigenvalues,

$$(3.3) \qquad \lambda_\pm = \frac{1}{2}\left[\mathrm{Tr}M \pm \sqrt{(\mathrm{Tr}M)^2 - 4\mathrm{Det}M} \right],$$

we see that $\mathrm{Re}(\lambda_+) \geq \mathrm{Re}(\lambda_-)$.

In order for (U_-, V_-) to be linearly stable, it must be that $\mathrm{Tr}M = \lambda_- + \lambda_+ < 0$ for all k. For $2\beta > \alpha$ the trace of M is to leading order:

$$(3.4) \qquad -(k^2 + \delta^{2(\alpha-\beta)}\frac{a^2}{b^2} + \delta^\alpha a + \delta^{2\sigma}k^2 - \delta^\beta b) < 0,$$

where we have substituted the leading order expression from (2.2) for V_-. In order for this relation to hold for all k, it must be that either $2(\alpha - \beta) \leq \beta$ (with $a^2 < b^3$ being sufficient in the case of equality), or $\alpha \leq \beta$ (now, with $a > b$ in the case of equality). Since $\alpha, \beta \geq 0$, the latter inequality is satisfied automatically whenever the former holds. Hence, we know that

$$(3.5) \qquad 2\alpha \leq 3\beta$$

is the only new condition that needs to be satisfied in order for (U_-, V_-) to be linearly stable.

We now find explicit values, a_c and k_c, of the parameter a and the wavenumber k such that (U_-, V_-) is marginally stable. We will also see in the course of the proof below that the other trivial stationary state (U_+, V_+) does not satisfy the conditions for marginal stability, and that is why our focus below is exclusively on (U_-, V_-). See Figure 3.1a. Marginal stability at k_c is equivalent to the situation in which $\mathrm{Re}(\lambda_-) < 0$ for all k and $\mathrm{Re}(\lambda_+) < 0$ for all $k \neq \pm k_c$, $\mathrm{Re}(\lambda_+)|_{\pm k_c} = 0$ and $\frac{d}{dk}\mathrm{Re}(\lambda_+)|_{\pm k_c} = 0$. We have that $\mathrm{Det}\, M = \lambda_+ \cdot \lambda_-$. Thus, marginal stability occurs for a_c and k_c that satisfy:

1. $\mathrm{Det}\, M(k; a_c) \geq 0$ for all k,
2. $\mathrm{Det}\, M(\pm k_c; a_c) = 0$,
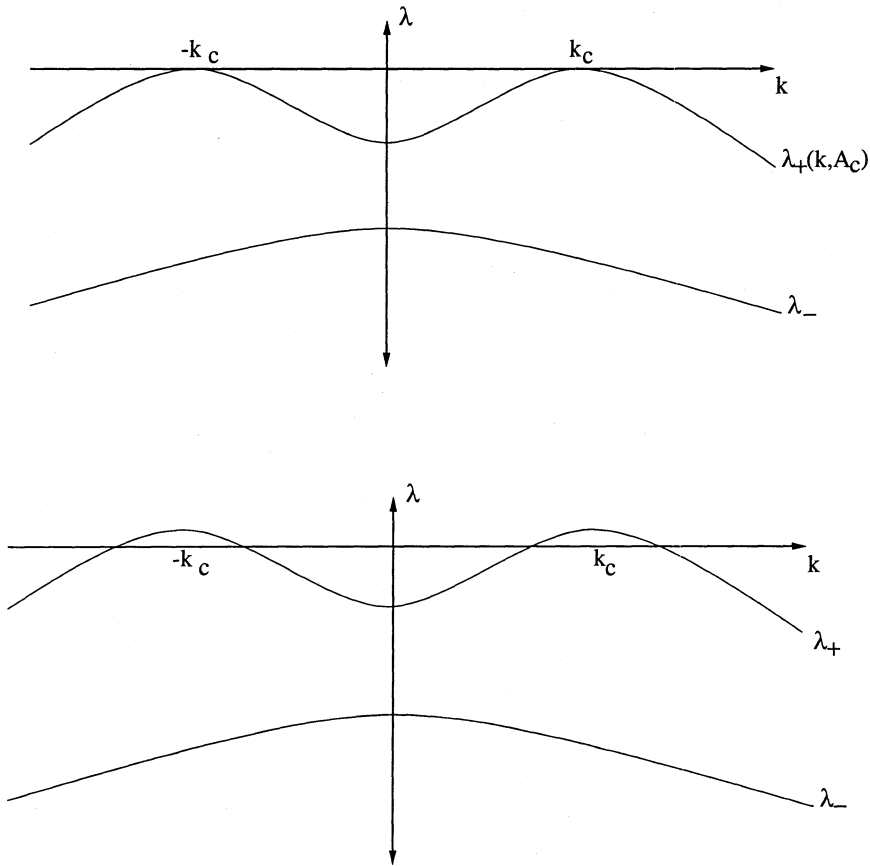3. $\frac{\partial}{\partial k}\mathrm{Det}\, M(\pm k_c; a_c) = 0$.

FIG. 3.1. **a.** *The $k - \lambda$ plane in the marginal stability case, where $A = A_c$.* **b.** *The $k - \lambda$ plane when $A < A_c$, $|A - A_c| \ll 1$.*

Condition 3 implies that locally (near $\pm k_c$) the eigenvalue curve λ_+ meets the k-axis in a quadratic tangency. We will now show:

PROPOSITION 3.1. *The stationary state (U_-, V_-) of (1.1) is marginally stable for*

$$\beta = \frac{2}{3}(\sigma + \alpha)$$
$$k_c^2 = \frac{(1 - g)b}{2\delta^{2(\beta - \alpha)}}$$
(3.6)
$$a_c^2 = gb^3,$$

to leading order, where $g = 3 - 2\sqrt{2}$.

Proof. Using condition 3, we obtain

(3.7)
$$k_c^2 = \frac{-(\delta^{2\sigma}V_-^2 + \delta^{2\sigma + \alpha}a_c - \delta^\beta b)}{2\delta^{2\sigma}}.$$

Also, using condition 2, we obtain an expression of the form

(3.8) $$k_c^2 f(k_c^2, \delta, a_c, b, V_-) = -\delta^\beta b(V_-^2 - \delta^\alpha a_c),$$

for some known function f. Substituting (3.7) for k_c^2 in f, we find

(3.9) $$k_c^2 = \frac{-2\delta^\beta b(V_-^2 - \delta^\alpha a_c)}{\delta^{2\sigma} V_-^2 + \delta^{2\sigma+\alpha} a_c - \delta^\beta b}.$$

Then, the requirement that k_c is real implies, using successively (3.7) and (3.9), the following additional conditions:

    4. $\delta^{2\sigma} V_-^2 + \delta^{2\sigma+\alpha} a_c - \delta^\beta b < 0$,
    5. $V_-^2 - \delta^\alpha a_c > 0$.

Since V_- only exists for $4B^2 < A$, and thus either $2\beta > \alpha$ or $2\beta = \alpha$ with $4b^2 > a$, we find by (2.2) and (1.2), respectively, that condition 5 is satisfied automatically. Thus, condition 4 is the only 'new' condition.

We now make a brief digression that is nevertheless part of the reason why the proposition is only stated for (U_-, V_-). In condition 5, if we replace the leading order expression for V_- with that for V_+, we obtain the condition:

(3.10) $$\delta^{2\beta-\alpha} b > a_c,$$

which cannot be satisfied when $2\beta > \alpha$ for $\delta \ll 1$, due to (2.7). Also, when $2\beta = \alpha$, it can be checked that $V_+^2 > \delta^\alpha a$. The equality, $V_\pm^2 = \delta^\alpha a = A$ (2.3) occurs at the bifurcation $a = 4b^2$ (or $A = 4B^2$) where $V_+ = V_-$. Thus, the other nontrivial homogeneous state (U_+, V_+) cannot be marginally stable, and that is why we focus only on (U_-, V_-) in this proposition.

Returning to the analysis of the state (U_-, V_-), we first restrict our attention to the case in which $2\beta > \alpha$. The other case $2\beta = \alpha$ is then treated at the end of the proof. Rewriting condition 4 using (2.2), one obtains to leading order:

(3.11) $$\frac{a_c^2}{b^2} \delta^{2(\alpha-\beta+\sigma)} + \delta^{2\sigma+\alpha} a_c - \delta^\beta b < 0.$$

Now $2\beta > \alpha$ implies that $\delta^{2\sigma+\alpha} a_c \ll \delta^{2(\alpha-\beta+\sigma)} \frac{a_c^2}{b^2}$. Thus, for the condition (3.11) to hold, one needs:

(3.12) $$\beta \le 2(\alpha - \beta + \sigma).$$

This, together with (3.5), implies:

(3.13) $$\sigma \ge 0.$$

Now, the inequalities in (3.5) and (3.12) imply that, to leading order, (3.7) is $\mathcal{O}(\delta^{\beta-2\sigma})$, while (3.9) is $\mathcal{O}(\delta^{2\alpha-2\beta})$. Thus, since (3.7) and (3.9) must be equal, we find:

(3.14) $$\beta = \frac{2}{3}(\alpha + \sigma).$$

Using this, we see that condition 4, as given by (3.11), becomes:

(3.15) $$a_c^2 < b^3.$$

Substituting the leading order expression (2.2) into the right-hand sides of (3.7) and (3.9), we find that to leading order

$$(3.16) \qquad \left(\frac{a_c^2}{b^3} - 1 \right)^2 = 4 \frac{a_c^2}{b^3}.$$

Finally, solving for a_c^2 and using condition (3.15), we obtain the desired formula, (3.6), for a_c. And, substituting this back into (3.7), we obtain the second line of (3.6). This concludes the proof for the case $2\beta > \alpha$.

When $\alpha = 2\beta > 0$ we see that the leading order term in is the trace of the matrix M (3.2) is $+\delta^\beta b$: $\mathrm{Tr} M$ cannot be negative for small k (note that we cannot use (3.4) since that approximation uses $2\beta > \alpha$). Thus, marginal stability can only occur for $\alpha = 2\beta = 0$. Substituting this in (3.7) and (3.9), we observe that these expressions for k_c can only be of the same magnitude when also $\sigma = 0$. Since we cannot use the leading order approximation (2.2) of (U_-, V_-) in this case, the above marginal stability calculations will be much more technical. Moreover, a degeneration will occur as $A \approx 4B^2$ (see Remark 3.1), therefore we do consider the details of this case.

COROLLARY 3.2. *For a slightly larger than a_c, (U_-, V_-) is linearly stable, and for a less than a_c, (U_-, V_-) is linearly unstable.*

Proof. For $2\beta > \alpha$ we have to leading order:

$$(3.17) \quad \frac{\partial}{\partial a} \mathrm{Det} \mathcal{M}|_{a=a_c} = 2 \frac{a_c k^2}{b^2} \delta^{2(\alpha - \beta + \sigma)} + 2 \frac{a}{b} \delta^{2\alpha - \beta} + \delta^{\alpha + 2\sigma} k^2 - \delta^{\alpha + \beta} b > 0,$$

since, in particular, $2\alpha - \beta < \alpha + \beta$. In addition, note that because $\lambda_+(a_c) = 0$, the product rule directly gives:

$$(3.18) \qquad \frac{\partial}{\partial a} \mathrm{Det} \mathcal{M}|_{a=a_c} = \frac{\partial}{\partial a} [\lambda_-(a) \cdot \lambda_+(a)] = \frac{\partial \lambda_+}{\partial a}|_{a=a_c} \cdot \lambda_-(a_c).$$

Finally, since $\lambda_-(a_c) \leq \lambda_+(a_c) = 0$, (3.17) implies that

$$(3.19) \qquad \frac{\partial \lambda_+}{\partial a}|_{a=a_c} < 0.$$

Therefore, the corollary is proven in the case $2\beta > \alpha$. The result for $\beta = \alpha = \sigma = 0$ can be obtained along the same lines.

3.2. The Eckhaus bands of stable periodic states: $|a - a_c| \ll 1$. We now turn our attention to the case with $a < a_c$, with $|a - a_c| \ll 1$. By the results from subsection 3.1, there exists a narrow band of wave numbers such that the homogeneous state (U_-, V_-) is unstable in this regime. See Figure 3.1b. For simplicity, we only consider the case $2\beta > \alpha$ (see Remark 3.1).

Heuristically, the idea is to derive a tractable equation, the Ginzburg-Landau equation, which will govern the behavior of the weakly-unstable solution (U_-, V_-), for $|a - a_c| \ll 1$. In particular, we will consider $a = a_c - \gamma^2$, where $0 < \gamma^2 \ll 1$ is a new small parameter.

We construct a small perturbation of (U_-, V_-). Using (2.2), and recalling that we are considering the case $2\beta > \alpha$, we define (U_-, V_-) implicitly via:

$$U_- = \delta^{2\beta - \alpha} \hat{U}_-$$

(3.20)
$$V_- = \delta^{\alpha-\beta}\hat{V}_-.$$

Setting $a = a_c - \gamma^2$ in the leading order expressions for $(\hat{U}_-, \hat{V}_-)$, where a_c is given in Proposition 3.1, we then substitute

(3.21)
$$U = \delta^{2\beta-\alpha}(\hat{U}_- + \gamma\hat{U}(x,t))$$
$$V = \delta^{\alpha-\beta}(\hat{V}_- + \gamma\hat{V}(x,t)),$$

into the Gray-Scott PDE (1.1) and rescale via $\tilde{x} = x\delta^{\beta-\alpha}$ and $\tilde{t} = \delta^\beta t$ to obtain the leading order system:

$$\delta^{3\beta-2\alpha}\frac{\partial U}{\partial t} = \frac{\partial^2 U}{\partial x^2} - b[gU + 2V] - \gamma\sqrt{\frac{b}{g}}\left[2gUV + V^2\right] - \gamma^2\left[UV^2 - 2\sqrt{\frac{g}{b}}U\right]$$

(3.22)
$$\frac{\partial V}{\partial t} = \delta^{2\sigma+2\alpha-3\beta}\frac{\partial^2 V}{\partial x^2} + b[gU + V] + \gamma\sqrt{\frac{b}{g}}\left[2gUV + V^2\right] + \gamma^2\left[UV^2 - 2\sqrt{\frac{g}{b}}U\right],$$

where we have dropped all of the hats and tildes from all variables. Finally, we recall that α, β and σ satisfy (3.12) (*i.e.* $2\sigma + 2\alpha - 3\beta = 0$), so that the coefficient on $\partial^2 V/\partial x^2$ is identically one. Moreover, the coefficient on $\partial U/\partial t$ is $\delta^{2\sigma} \ll 1$ and can thus be ignored to leading order.

If we neglect the $\mathcal{O}(\gamma)$ terms, we will recover the rescaled linear stability problem. The eigenvalue problem is

(3.23)
$$\det\begin{pmatrix} -bg - k^2 - \delta^{3\beta-2\alpha}\lambda & -2b \\ bg & b - k^2 - \lambda \end{pmatrix} = 0.$$

Note that $k_c^2 = \frac{1}{2}(1-g)b$, which is obtained from (3.6) through the above rescaling for x. Define

(3.24)
$$\mathcal{M}_c \equiv \begin{pmatrix} -\frac{1}{2}(1+g) & -2 \\ g & \frac{1}{2}(1+g) \end{pmatrix},$$

and note that $\mathcal{M}_c$ is nilpotent. The kernel of $\mathcal{M}_c$ is given by

$$\mathcal{S} = \text{span} < \begin{pmatrix} 2 \\ -\frac{1}{2}(1+g) \end{pmatrix} >,$$

where we recall that $g = 3 - 2\sqrt{2}$. Thus, since $\mathcal{M}_c$ is nilpotent, $\mathcal{M}_c\mathbf{x} = \mathbf{c}$ has a solution if $\mathbf{c} \in \mathcal{S}$. In this way, we obtain an orthogonality condition:

(3.25)
$$\frac{1}{2}(1+g)c_1 + 2c_2 = 0,$$

where $\mathbf{c} = (c_1, c_2)^T$, which will be central to the procedure below for deriving the Ginzburg-Landau equation.

The idea of deriving a modulation equation, such as here the Ginzburg-Landau equation, is that the solution (U, V) of (3.22) must be 'close' to the critical solution of the linear $\mathcal{O}(1)$ problem:

(3.26)
$$\begin{pmatrix} U \\ V \end{pmatrix} = \mathcal{A}(\xi, \tau)\begin{pmatrix} 2 \\ -\frac{1}{2}(1+g) \end{pmatrix} e^{ik_c x} + \text{c.c.} + \text{h.o.t.},$$

where $\mathcal{A}(\xi, \tau)$ is an amplitude term that depends on the slow time $\tau = \gamma^2 \tilde{t}$ and rescaled spatial variable $\xi = \gamma \tilde{x}$, and c.c. denotes the complex conjugate. Thus, if one knows the behavior of $\mathcal{A}$, then one knows the behavior of the solutions (U, V) of (3.22).

The Ginzburg-Landau equation is an equation for $\mathcal{A}(\xi, \tau)$. For the Gray-Scott problem, we find to leading order, in both δ and γ:

$$(3.27) \qquad \mathcal{A}_\tau = \frac{2}{\sqrt{b}} \mathcal{A} + 2\sqrt{2} \mathcal{A}_{\xi\xi} - \frac{2}{9}(10\sqrt{2} - 7)|\mathcal{A}|^2 \mathcal{A}.$$

The derivation of this equation is given in Appendix A. The so-called Landau coefficient in front of the cubic term in (3.27) is negative. Thus, one can explicitly find the band of periodic solutions to (3.27) by setting $\mathcal{A}(\xi, \tau) = Re^{i\kappa\xi}$, where R is a constant. Substituting this into (3.27), one obtains a cubic for R. Nontrivial solutions R and κ are given by the following equation:

$$(3.28) \qquad \kappa^2 + \frac{1}{18}(20 - 7\sqrt{2})R^2 = \frac{1}{\sqrt{2b}}.$$

A straightforward linear stability analysis shows that none of the solutions within this band satisfying

$$(3.29) \qquad |\kappa| < \frac{1}{(2b)^{1/4}\sqrt{3}},$$

have spectrum on the right hand side of the imaginary axis (the solutions outside this band have a piece of unstable (continuous) spectrum, see [36]). Hence, all of the solutions within this band that satisfy (3.29) are linearly stable. However, the continuous spectrum of the periodic solutions in this subband reaches up to the imaginary axis, therefore one cannot expect these solutions to be stable in a very strong sense, as we shall see in subsection 3.3.

REMARK 3.1. There is an additional complication in the case $\alpha = \beta = \sigma = 0$. Since $a = A$ then, and moreover $V_-^2 = V_+^2$ when $A = 4B^2$, by (1.2), it follows from (3.9) that $k_c \downarrow 0$ as $a = A \downarrow 4B^2$. As a consequence, one cannot use the above standard Ginzburg-Landau approach to study the weakly nonlinear stability of (U_-, V_-) for $A \approx 4B^2$, since the Fourier decomposition breaks down (see (3.26) and (A.1) in Appendix A). This degeneration in the Ginzburg-Landau equation has been studied in detail in [32]. It has been shown there that in this case the Ginzburg-Landau equation transforms in a rather singular fashion into the so-called extended Fisher-Kolmogorov equation. This has a drastic influence on the existence, stability and type of the (periodic) solutions that appear at this bifurcation. Note that in the context of the linearized stability analysis in the ODE for the spatial dynamics (as in Section 2), this degeneration corresponds to an eigenvalue $\lambda = 0$ of multiplicity 4. In this paper, we do not intend to go into the details of this special case. Note that in the simulations in Section 6 we will always consider $\sigma > 0$ (as in most simulations of the Gray-Scott model), thus we do not come close to the case $\alpha = \beta = \sigma = 0$.

3.3. Nonlinear diffusive stability.

The outcome of the asymptotic analysis on the stability of the small amplitude spatially periodic solutions in subsection 3.2 can be validated by applying the results of Schneider [33], [34] to this situation. In particular, we show in this subsection that Theorem 1.1 of Schneider [34] may be

used to justify the stability result (3.29). This theorem applies to reaction-diffusion equations of the form

$$(3.30) \qquad\qquad \mathbf{U}_t = \mathcal{A}\mathbf{U} + \mathbf{F}(\mathbf{U}),$$

where $x \in \mathbb{R}^d$, $t \geq 0$, $\mathbf{U}(x,t) \in \mathbb{R}^{\tilde{d}}$, $\mathcal{A} = \text{diag}(a_1\Delta, \ldots, a_{\tilde{d}}\Delta)$ with $a_j > 0$ for $j = 1, \ldots, d$ and $\mathbf{F}$ is at least C^4. The Gray-Scott model (1.1) clearly belongs to this class of systems with $d = 1$ and $\tilde{d} = 2$. There are two essential assumptions in the statement of this theorem: (*i*) there should exist a spatially periodic equilibrium solution $\mathbf{U}(x,t) = \mathbf{U}_p(x)$ of (3.30) and (*ii*) the periodic pattern $\mathbf{U}_p(x)$ should be spectrally stable, *i.e.*, the linearized stability problem should have no spectrum to the right of the imaginary axis. Note that $\lambda = 0$ must be in the spectrum due to the translational invariance.

The perturbations $\mathbf{V}(x,t) = \mathbf{U}(x,t) - \mathbf{U}_p(t)$ of the spatially-periodic state $\mathbf{U}_p(x)$ satisfy the equation

$$(3.31) \qquad\qquad \mathbf{V}_t = [\mathcal{A} + \mathbf{D_U}\mathbf{F}(\mathbf{u}_p)]\,\mathbf{V} + \mathbf{N}(\mathbf{V}).$$

Theorem 1.1 in [34] then states that, if both assumptions (*i*) and (*ii*) are satisfied, sufficiently small perturbations $\mathbf{V}(x,t)$ of the periodic solution $\mathbf{U}_p(x)$ decay algebraically in time (in a particular weighted Sobolev space):

THEOREM 3.1 (Schneider [34]). *Let $\tilde{\delta} > 0$. Assume that the system (3.30) has a spectrally stable, stationary, spatially-periodic solution $\mathbf{U}(x,t) = \mathbf{U}_p(x)$. Let $\mathbf{V}_0$ be an initial condition of (3.31) with $\mathbf{V}_0\rho \in H^{d/2+\tilde{\delta}}(\mathbb{R}^d)$, where $\rho(x) = (1 + |x|^2)^d$. There exist positive constants C_1 and C_2 such that if $\|\mathbf{V}_0\rho\|_{H^{d/2+\tilde{\delta}}(\mathbb{R}^d)} \leq C_1$, then the solution $\mathbf{V}$ of (3.31) with $\mathbf{V}|_{t=0} = \mathbf{V}_0$ exists for all $t \geq 0$ and satisfies $\|\mathbf{V}(t)\|_{L^\infty(\mathbb{R}^d)} \leq C_2(1 + t)^{-d/2}$.*

This result generalizes the stability properties of the periodic solutions of the Ginzburg-Landau equation (see for instance [22]) to stationary periodic patterns that appear at bifurcations in reaction-diffusion systems that can be approximated by a Ginzburg-Landau equation, as we did in subsection 3.2 using the asymptotic methods. Hence, if we can show that both assumptions (*i*) and (*ii*) are satisfied, we may conclude by this theorem that the solutions inside the parabola (3.29) are diffusively stable.

There is a straightforward procedure to check that the analysis in the previous subsections implies that these assumptions hold for the solutions described by (3.29), however, we do not go into the details here. The existence of the solutions described by (3.28) is only shown in an asymptotic leading order sense, the rigorous justification can be established by appealing to the results of [19] and [20]. The linear stability analysis of these solutions is performed through the simplification of using the Ginzburg-Landau formalism. The linearized stability results found in the previous subsection through this asymptotic procedure show that condition (*ii*) is satisfied for those periodic patterns that satisfy (3.29). Thus, we can conclude:

THEOREM 3.2. *Let $A = a\delta^\alpha = (a_c - \gamma^2)\delta^\alpha$ where a_c is given by (3.6) and let $\beta = \frac{2}{3}(\sigma + \alpha) > 0$. For $0 < \gamma \ll 1$ small enough (independent of δ), there exists a 1-parameter family of stationary spatially-periodic solutions of (1.1) that are close to the stationary state (U_-, V_-) (1.2):*

$$\begin{pmatrix} U(x;\kappa) \\ V(x;\kappa) \end{pmatrix} = \begin{pmatrix} U_- \\ V_- \end{pmatrix} + \gamma Re^{i(k_c+\gamma\kappa)\delta^{\beta-\alpha}x}\begin{pmatrix} 2\delta^{2\beta-\alpha} \\ -(2-\sqrt{2})\delta^{\alpha-\beta} \end{pmatrix} + \text{c.c.} + \text{h.o.t.}$$
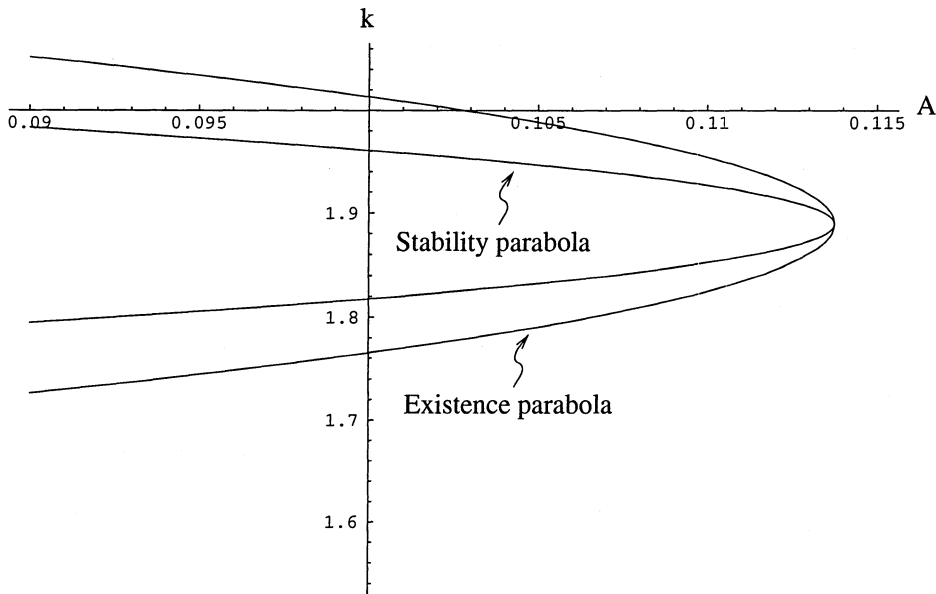
FIG. 3.2. *The existence and stability parabolas near $A = A_c$ plotted in the $A - k$ plane, as obtained from the leading order perturbation analysis carried out in Section 3. Here the following choice of parameters is made in order to graph the analytically obtained functions: $A_c = a_c \delta^\alpha$, $B = b\delta^\beta$, $D_U = 1.0$ and $D_V = 0.01$, where $a_c = 0.114$, $b = 0.4$, $\delta = 0.1$, $\alpha = 0$, $\beta = 2/3$, and $\sigma = 1$. The stability parabola marks the upper tip of the Busse balloon that will be found in Section 6.*

where R and κ are related by (3.28) and k_c is given by (3.6). Moreover, the solutions with κ satisfying (3.29) are diffusively stable in the sense of Theorem 3.1.

REMARK 3.2. The unscaled period of these solutions is given by $2\pi\delta^{\alpha-\beta}/(k_c + \gamma\kappa)$ which is $\mathcal{O}(1)$ by (3.6). See Figure 3.2 for plots of the existence and stability parabolas in the $A - k$ plane corresponding to these orbits.

4. Existence of stationary, spatially-periodic solutions: $\beta < \frac{2}{3}(\sigma + \alpha)$. In this section, we establish the conditions under which (2.4) has periodic orbits when A is much less than the critical parameter A_c. The precise results are stated in Theorems 4.1 and 4.3 below. Also, we will set $t = \hat{\eta}$ and refer to t as time, since we work with the system (2.4) as a dynamical system, and we recall that we have dropped hats.

Let $(u(0), p(0), v(0), q(0))$ denote an initial condition for (2.4). In particular, we consider initial conditions with $p(0) = 0$, $q(0) = 0$ and $v(0) > b/u(0)$. Let $T_{\epsilon,1}$ ($-T_{\epsilon,2}$) denote the forward (backward) time taken for the solution with initial condition $(u(0), 0, v(0), 0)$ to intercept the $\{q = 0\}$ hyperplane for the first time. In view of the symmetry (2.6), it must be the case that:

$$(u, p, v, q)|_{-T_{\epsilon,2}} = (u, p, v, q)|_{T_{\epsilon,1}},$$

in order for the orbit $(u(t), p(t), v(t), q(t))$ through these initial conditions to be periodic. See Figures 2.1 and 2.2. Moreover, since any periodic orbit of (2.4) with this

type of initial condition must satisfy the symmetry (2.6), $T_{\epsilon,2} = T_{\epsilon,1}$. We denote this time by T_ϵ.

The condition that $v(-T_\epsilon) = v(T_\epsilon)$ can be reexpressed using the Hamiltonian K and the fact that $q(\pm T_\epsilon) = 0$. In particular, a periodic orbit exists if the following relations hold:

$$\Delta K(K_0, u_0, p_0) \equiv \int_{-T_\epsilon}^{T_\epsilon} \dot{K}(u, p, v, q)dt = 0$$

$$\Delta u(K_0, u_0, p_0) \equiv \int_{-T_\epsilon}^{T_\epsilon} \dot{u}(u, p, v, q)dt = 0$$

(4.1) $$\Delta p(K_0, u_0, p_0) \equiv \int_{-T_\epsilon}^{T_\epsilon} \dot{p}(u, p, v, q)dt = 0,$$

where $u_0 = u(0)$ and $p_0 = 0$ for our choice of initial conditions, and K_0 is the value of the Hamiltonian at the initial condition $(v, q) = (v(0), 0)$.

To analyze the condition involving ΔK, we differentiate the Hamiltonian K, given by (2.12), along trajectories of (2.4) and treating u as a constant:

$$\Delta K(K_0, u_0, p_0) = \frac{\epsilon}{3} \int_{-T_\epsilon}^{T_\epsilon} pv^3 dt.$$

The symmetry (2.6) implies that the solution through an initial condition with $p(0) = p_0 = 0$ and $q(0) = 0$ satisfies the relation $p(-t) = -p(t)$, as well as the condition $v(-t) = v(t)$. Thus, the integrand is an odd function, and the requirement that $\Delta K = 0$ is automatically satisfied by the orbits through $(u(0), 0, v(0), 0)$ for any $u(0) > 0$ and $v(0) > b/u(0)$.

To analyze the condition involving Δu, we use (2.4)(a) to rewrite the integral in (4.1) as:

$$\Delta u(K_0, u_0, p_0) = \epsilon \int_{-T_\epsilon}^{T_\epsilon} p \ dt.$$

Again, symmetry (2.6) implies that the solution through an initial condition with $p(0) = p_0 = 0$ and $q(0) = 0$ satisfies the relation $p(-t) = -p(t)$. Therefore, since the interval of integration is symmetric about $t = 0$, we see that the requirement of $\Delta u = 0$ for having a periodic orbit is also satisfied automatically by the orbit through the initial condition $(u(0), 0, v(0), 0)$ for any $u(0)$ and $v(0) > b/u(0)$.

In the next two subsections, we will analyze the condition $\Delta p = 0$ and complete the proof of the existence of periodic orbits. In subsection 4.1, we examine the case $2\beta - \alpha > 0$ ($\rho > 0$, recall (2.5)), while in subsection 4.2, we treat the case $2\beta - \alpha = 0$ ($\rho = 0$).

4.1. Analysis of Δp for $\rho > 0$.

THEOREM 4.1. *For $\rho > 0$ (i.e. for $2\beta - \alpha > 0$), $\beta < 2/3(\sigma + \alpha)$, for all positive and $\mathcal{O}(1)$ values of a and b, and for each $0 < u_0 < b^2/a$, there exists a $v(0; u_0) > b/u_0$ such that the system (2.4) has a periodic orbit with initial condition of the form $(u_0, 0, v(0; u_0), 0)$.*

Proof. As we have already shown, the conditions that $\Delta u = 0$ and $\Delta K = 0$ are satisfied by the trajectories through $(u(0), 0, v(0), 0)$ for all a, b and $u(0) > 0$, and for all $v(0) > b/u(0)$. Thus, we will complete the proof by analyzing when Δp vanishes.

From (2.4) and (2.6), one may directly compute:

$$(4.2) \qquad \Delta p(K_0, u_0, p_0) = 2\epsilon \int_{-T_\epsilon}^{0} [uv^2 - a + \epsilon^\rho au] dt.$$

In order to estimate $u(t)$, we recall that $\dot{u} = \epsilon p$. Since $p(0) = 0$, since T_ϵ is bounded above by an $\mathcal{O}(\log(1/\epsilon))$ quantity, and since $\dot{p} = \mathcal{O}(\epsilon)$, we know that $p(t) = \mathcal{O}(\epsilon)$ for $t \in [0, C \log(1/\epsilon))$, and hence u is constant ($= u_0$) to leading order.

Let T_0 be the time taken for the unperturbed solution of the fast system with $u = u_0$ and with initial condition $(v, q) = (v(0), 0)$ to intercept the $\{q = 0\}$ hyperplane the first time. It follows that to leading order:

$$(4.3) \qquad \Delta p(K_0, u_0, p_0) = 2\epsilon \int_{-T_0}^{0} (u_0 v^2 - a) dt,$$

since $\epsilon^\rho au$ is a higher order term, when $\rho > 0$.

We will show that for $a, b = \mathcal{O}(1)$, there is a unique initial condition of the form $(u_0, 0, v(0), 0)$ with $u_0 > 0$ and $v(0) > b/u_0$, such that $\Delta p = 0$. We will do this via a monotonicity argument which shows that, in the limit $\epsilon \to 0$, Δp varies monotonically as $v(0)$ increases from b/u_0, the value at the center fixed point of the fast subsystem, to $3b/2u_0$, the value at the point where the orbit homoclinic to ($v = 0, q = 0$) intersects the v-axis. Moreover, zero is contained inside the interval over which Δp varies, and this together with monotonicity and a straightforward application of the Implicit Function Theorem implies the desired result.

As a preliminary step to establish monotonicity, we will rework the expression for Δp. The procedure we employ follows that also used in [5]. Using the Hamiltonian (2.12) and the first equation of the fast v-q subsystem of (2.4) for $q > 0$, one has:

$$(4.4) \qquad \frac{dv}{dt} = \pm\sqrt{2K + bv^2 - \frac{2}{3}uv^3}.$$

For clarity, let $G_K(v; u, b) \equiv 2K + bv^2 - \frac{2}{3}uv^3$. Changing variables of integration in (4.3) from t to v, we obtain

$$(4.5) \qquad \Delta p(K_0, u_0, p_0) = 2\epsilon \int_{v_{min}}^{v_{max}} \frac{u_0 v^2 - a}{\sqrt{G_K(v; u_0, b)}} dv,$$

where v_{min} and v_{max} are the points of intersection of the unperturbed periodic orbit of energy K_0 with the positive v-axis. See Figure 2.1.

The expression for Δp may be further analyzed by defining:

$$(4.6) \qquad T_i(K) \equiv \oint \frac{v^i dv}{\sqrt{G_K(v; u_0, b)}},$$

where the contour is taken in the complex plane around the real interval $[v_{min}, v_{max}]$. Then, since the integral of a derivative on a closed contour is zero, one has, for $j \geq 1$:

$$0 = \oint \frac{d}{dv}(v^{j-1}\sqrt{G_K(v; u_0, b)}) dv$$

$$(4.7) \qquad = (j-1)\oint v^{j-2}\sqrt{G_K(v; u_0, b)} dv + bT_j - u_0 T_{j+1}.$$

It follows that when $j = 1$, the first term of the second equation on the right hand side of (4.7) vanishes, and we have

$$(4.8) \qquad T_2 = \frac{b}{u_0} T_1.$$

Thus, to leading order, we have:

$$(4.9) \qquad \frac{\Delta p(K_0, u_0, p_0)}{\epsilon} = u_0 T_2(K) - a T_0(K) = b T_1(K) - a T_0(K).$$

The monotonicity of Δp will now follow from monotonicity of the ratio T_1/T_0. So, let

$$(4.10) \qquad \tau(K; u_0, a, b) \equiv \frac{T_1(K)}{T_0(K)}.$$

We want to show that for a, $b = \mathcal{O}(1)$, there is an initial condition of the form $(u_0, 0, v(0), 0)$ whose orbit has energy K in the fast subsystem, such that

$$(4.11) \qquad \tau(K; u_0, a, b) = \frac{a}{b}.$$

In particular, we will show that one can find a $v(0)$ such that (4.11) holds and τ is monotonically decreasing as v passes through this value, for every $u_0 \leq \frac{b^2}{a}$, by establishing:

PROPOSITION 4.2. Let $K_c = -\frac{b^3}{6u^2}$ denote the energy of the center $(\frac{b}{u}, 0)$ of the unperturbed v-q subsystem, and note that the energy of the saddle $(0,0)$ is 0. Then

$$(i) \lim_{K \downarrow K_c} \tau(K) = \frac{b}{u},$$
$$(ii) \lim_{K \uparrow 0} \tau(K) = 0,$$
$$(iii) \frac{d}{dK} \tau(K) < 0 \qquad \text{for } K \in (K_c, 0).$$

REMARK 4.1. Note that as $u_0 \to \frac{b^2}{a}$, from condition (i) we have that $\lim_{K \downarrow K_c} \tau(K) = \frac{a}{b}$, the requirement of (4.11). Thus, the periodic orbit we find in this limit occurs when $K = K_c$, which implies that $v(0) = \frac{a}{b}$, and the periodic orbit collapses to the homogeneous state (U_-, V_-). The other limit, $u_0 \to 0$, will be studied in Section 5.

Proof. First, we evaluate the limits of T_0 and T_1 as $K \to K_c$ and as $K \to 0$, the energy at the center and saddle, respectively. Taking the limit inside the integral, expanding the resulting expression about $v = \frac{b}{u}$ and integrating with the residue theorem, we find

$$(4.12) \qquad \lim_{K \downarrow K_c} T_0(K) = \frac{2\pi}{\sqrt{b}}, \qquad \lim_{K \downarrow K_c} T_1(K) = 2\pi \frac{\sqrt{b}}{u}.$$

Next, by taking the limit inside the integral and evaluating the integral directly, one also has:

$$(4.13) \qquad \lim_{K \uparrow 0} T_0(K) = \infty, \qquad \lim_{K \uparrow 0} T_1(K) = \frac{6\sqrt{b}}{u}.$$

Thus, using the definition of τ given in (4.10), (*i*) and (*ii*) are proven.

Finally, we show that $\tau(K; u, a, b)$ is monotone in K. This will be achieved by showing that $d\tau/dK < 0$ for $K \in (K_c, 0)$. In particular,

$$(4.14) \quad \frac{d\tau}{dK} = \frac{d}{dK}\left(\frac{T_2(K)}{T_0(K)}\right) = \frac{d}{dK}\left(\frac{b}{u}\frac{T_1(K)}{T_0(K)}\right) = \frac{b}{u}\left[\frac{-T_0(K)J_1(K) + T_1(K)J_0(K)}{T_0^2(K)}\right].$$

where

$$(4.15) \quad J_i(K) \equiv \oint \frac{v^i}{G_K(v; u, b)\sqrt{G_K(v; u, b)}} dv$$

and, for $i \geq 0$:

$$(4.16) \quad \frac{d}{dK}T_i(K) = -J_i(K).$$

From this we observe that we only need J_0 and J_1 to calculate $d\tau/dK$. However, we need equations for $J_0, \ldots, J_4$ in order to evaluate J_0 and J_1 in terms of T_0 and T_1. Through straightforward manipulations one finds that:

$$
\begin{aligned}
T_0 &= \oint \frac{G_K(v; u, b)}{G_K(v; u, b)\sqrt{G_K(v; u, b)}} dv = 2KJ_0 + bJ_2 - \frac{2}{3}uJ_3, \\
(4.17) \quad T_1 &= \oint \frac{vG_K(v; u, b)}{G_K(v; u, b)\sqrt{G_K(v; u, b)}} dv = 2KJ_1 + bJ_3 - \frac{2}{3}uJ_4.
\end{aligned}
$$

Also,

$$(4.18) \quad 0 = \oint \frac{d}{dv}\left(\frac{v^{(j-1)}}{\sqrt{G_K(v; u, b)}}\right) dv = (j-1)T_{j-2} - bJ_j + uJ_{j+1}$$

for $j \geq 1$. Now take $j = 1, 2, 3$ in (4.18) to find three additional equations. Thus, (4.17)-(4.18) constitute a 5×5 linear system in the unknowns $J_0, \ldots, J_4$:

$$(4.19) \quad \begin{pmatrix} 2K & 0 & b & -\frac{2}{3}u & 0 \\ 0 & 2K & 0 & b & -\frac{2}{3}u \\ 0 & b & -u & 0 & 0 \\ 0 & 0 & b & -u & 0 \\ 0 & 0 & 0 & b & -u \end{pmatrix} \begin{pmatrix} J_0 \\ J_1 \\ J_2 \\ J_3 \\ J_4 \end{pmatrix} = \begin{pmatrix} T_0 \\ T_1 \\ 0 \\ T_0 \\ 2T_1 \end{pmatrix}.$$

Solving this system, we find that

$$
\begin{aligned}
J_0 &= \frac{6Ku^2T_0 + b^2uT_1}{6K(b^3 + 6Ku^2)}, \\
(4.20) \quad J_1 &= \frac{buT_0 - u^2T_1}{b^3 + 6Ku^2}.
\end{aligned}
$$

Thus, plugging these solutions (4.20) into (4.14), we find that

$$(4.21) \quad \frac{d\tau}{dK} = \frac{b^2\tau^2 + 12uK\tau - 6Kb^2}{6K(b^3 + 6Ku^2)}.$$

For $K \in (K_c, 0)$, note that the discriminant of the quadratic $\mathcal{Q}(\tau) = b\tau^2 + 12uK\tau - 6Kb^2$ is 0 at $K = K_c$ and at $K = 0$, and is negative for $K \in (K_c, 0)$. Combined with

the fact that $\mathcal{Q}(0) > 0$, this implies that $Q > 0$ for all τ. Since the denominator is negative for all $K \in (K_c, 0)$, we conclude that:

$$(4.22) \qquad \frac{d\tau}{dK} < 0.$$

This concludes the proof of the proposition, and the analysis for $\delta = 0$ ($\epsilon = 0$).

A straightforward application of the Implicit Function Theorem shows that, when $0 < \delta \ll 1$ ($0 < \epsilon \ll 1$), the higher order terms in the asymptotic expansion do not structurally alter the results obtained from the leading order analysis. Thus, the proof of the theorem follows.

4.2. Analysis of Δp for $\rho = 0$. In this subsection, we consider the case where $\rho = 0$ (*i.e.* $2\beta - \alpha = 0$), and again we assume $\beta < 2/3(\sigma + \alpha)$. The analysis proceeds in a fashion similar to that used in subsection 4.1. From (2.4) and (2.6) we have

$$(4.23) \qquad \Delta p(K_0, u_0, p_0) = 2\epsilon \int_{-T_\epsilon}^0 [uv^2 - a + au]dt.$$

The leading order integral is

$$(4.24) \qquad \Delta p(K_0, u_0, p_0) = 2\epsilon \int_{-T_0}^0 [u_0 v^2 - a(1 - u_0)]dt,$$

where we now need to keep the third term in the integrand, since it is no longer of higher order.

Following the same steps as in subsection 4.1, we obtain a condition similar to (4.11):

$$(4.25) \qquad \tau(K; u_0, a, b) = \frac{a}{b}(1 - u_0)$$

As with (4.11), if this condition is satisfied for some initial condition $(u_0, 0, v(0), 0)$, for which the orbit in the fast subsystem has energy K, then $\Delta p = 0$ and a periodic orbit exists. Note that the results of Proposition 4.2 carry over without modification in this case. Thus, for (4.25) to hold, we have, using the condition (*i*) of Proposition 4.2, the requirement that

$$(4.26) \qquad \frac{b}{u_0} \geq \frac{a}{b}(1 - u_0).$$

Since $\tau \geq 0$, we need to require that $0 < u_0 < 1$. Note that the boundaries of the u_0 region defined by (4.26) are given by the trivial stationary states $u_0 = U_\pm$ (1.2). Thus, for $4b^2 \leq a$ (or equivalently $4B^2 \leq A$, since $\alpha = 2\beta$), we arrive at the requirements that either $0 < u_0 < U_-$ or $U_+ < u_0 < 1$, while for $4b^2 > a$ we only need $0 < u_0 < 1$.

THEOREM 4.3. *Let $\rho = 0$ (i.e. $2\beta - \alpha = 0$) and $\beta < 2/3(\sigma + \alpha)$. For $\mathcal{O}(1)$ $a, b > 0$ such that $4b^2 \leq a$ there exists for all*

$$u_0 \in (0, U_-) \cup (U_+, 1)$$

a $v(0; u_0)$ such that the system (2.4) has a periodic orbit with initial condition of the form $(u_0, 0, v(0; u_0), 0)$, where $v(0; u_0) > b/u_0$. For $a, b > 0$ such that $4b^2 > a$ there exist periodic orbits of the same type for all

$$u_0 \in (0, 1).$$

The relation between Theorems 4.1 and 4.3 of this work may be seen as follows. Taking b smaller (*i.e.*$\ll 1$) in Theorem 4.3 is equivalent to taking β larger (*i.e.* $2\beta > \alpha$). Using the leading order approximation (2.2) of U_- and combining it with the scaling (2.3) of u shows that the interval $0 < u_0 < U_-$ coincides, to leading order, with the interval $0 < u_0 < b^2/a$ of Theorem 4.1 in this limit.

The new interval $(U_+, 1)$ remains $\mathcal{O}(1)$ when b becomes small. Due to the scaling (2.3) of u this means that this u interval is not of $\mathcal{O}(1)$ in the $\hat{u}$ scaling. As a consequence, we did not find these periodic solutions in the previous sections. However, one can recover these periodic solutions in a straightforward fashion by adapting the scalings of u and v to those of the state (U_+, V_+), instead of that of (U_-, V_-) as in (2.3): the second interval corresponds to periodic orbits centered around (U_+, V_+) (see also below). We do not consider this other scaling in any detail, since we have seen in Section 3 that the pattern $(U \equiv U_+, V \equiv V_+)$ cannot become marginally stable: there is no local mechanism by which these orbits can become stable. This also agrees with the fact that we do not observe any stable periodic orbits around (U_+, V_+) in numerical simulations.

The boundaries $u_0 \uparrow U_-$ and $u_0 \downarrow U_+$ both correspond to periodic orbits that 'shrink' into the fixed points corresponding to the trivial states $(U_\pm, V_\pm)$. The other two boundaries, $u_0 = 0$ and $u_0 = 1$, that persist as a decreases through $4b^2$, correspond to global bifurcations that have so far not been studied in any detail. In particular, the boundary $u_0 = 0$ has to be studied in a completely independent fashion since we assumed that $u_0 = \mathcal{O}(1)$ in this section. Also, when $\rho < 0$, the other boundary $u_0 = 1$ corresponds to $0 < u_0 \ll 1$. This can be seen immediately by checking formally that the condition $0 \leq \tau(K) \leq 1$ reduces to $0 \leq \tau \leq \epsilon^{-\rho}$ when ρ has become negative, see (2.4) and the derivation of $\tau(K)$ (4.25). Both of these global bifurcations will be studied in the next section by assuming that $0 < u_0 \ll 1$, and we shall see that they are singular in nature. See also subsection 5.4 for the case $\rho = 0$ and $u_0 \approx 1$.

REMARK 4.2. In Section 3, we deduced that the Ginzburg-Landau/Turing bifurcation can only occur for $\rho \geq 0$, and the main result was the existence of a family of periodic orbits with $\mathcal{O}(1)$ period that lie near the critical point. However, as we have just indicated, one can show (as we do in Section 5) that there also exist (singular) periodic orbits for $\rho < 0$ that are not close to a critical point. These orbits are interesting from a singular perturbation point of view, and they can become stable as has already been observed in [7].

5. Continuation of periodic states into the singular regime.
In this section, we prove the existence of a family of 'singular' stationary spatially-periodic solutions of (1.1) with $0 < u_0 \ll 1$. A periodic orbit of (2.4) in this regime of initial conditions is labeled singular because it has two distinct components: for 'most' of its period, its orbit lies near the slow manifold $\mathcal{M} = \{(u, p, v, q)|v, q = 0\}$, and for a brief time interval it makes an excursion into the fast field. By contrast, the orbits studied in Sections 3 and 4 lie exclusively in the fast field.

Further information, beyond that already given in Section 2, is needed about the slow manifold $\mathcal{M}$ for the analysis of this section. In particular, in order to prove the existence of periodic orbits with initial conditions $0 < u_0 \ll 1$, we will need to know the relative dispositions of the stable and unstable manifolds, $W^s(\mathcal{M})$ and $W^u(\mathcal{M})$, of $\mathcal{M}$ and about their intersections. Although the periodic orbits clearly do not lie in

$W^s(\mathcal{M}) \cap W^u(\mathcal{M})$, we will see that they are exponentially close to $W^s(\mathcal{M}) \cap W^u(\mathcal{M})$, just as those whose existence was shown in Theorem 4.2 of [6].

At the end of subsection 4.2 here, we showed that the singular periodic solutions can be found in the regime in which $0 < u_0 \ll 1$ for both $\rho > 0$ and $\rho < 0$. Therefore, we introduce an additional scaling of u ($= \hat{u}$):

$$(5.1) \qquad\qquad u = \epsilon^\nu \tilde{u},$$

where $\nu \geq 0$ and now $\tilde{u}$ is by definition $\mathcal{O}(1)$. Performing a scaling analysis similar to that carried out in Section 2, we obtain a rescaling of (2.4):

$$
\begin{aligned}
\dot{\tilde{u}} &= \epsilon^{1-\nu} p \\
\dot{p} &= \epsilon^{1-\nu}[\tilde{u}\tilde{v}^2 - a\epsilon^\nu(1 - \epsilon^{\rho+\nu}\tilde{u})] \\
\dot{\tilde{v}} &= \tilde{q} \\
(5.2) \qquad\qquad \dot{\tilde{q}} &= -\tilde{u}\tilde{v}^2 + b\tilde{v},
\end{aligned}
$$

where $v = \epsilon^{-\nu}\tilde{v}$, $q = \epsilon^{-\nu}\tilde{q}$, and p remains unscaled. Note that, as in Section 2, the scales of $\tilde{v}$ and $\tilde{q}$ are chosen such that the linear term and the nonlinear term are both $\mathcal{O}(1)$ in the equation for $\ddot{\tilde{v}} = \dot{\tilde{q}}$. This rescaling gives a definite lower bound on the magnitude of u_0:

$$(5.3) \qquad\qquad 0 < \nu < 1 \text{ or } u_0 \gg \epsilon,$$

since (5.2) can only be considered to be a singular system for these values of ν (see Remark 5.2).

REMARK 5.1. If we search in this equation for periodic solutions of the same type studied in Section 4, we arrive to leading order at

$$(5.4) \qquad\qquad \Delta p(\tilde{K}_0, \tilde{u}_0, p_0) = \epsilon^{1-\nu} b T_1(\tilde{K})$$

as the counterpart of (4.9), where $\tilde{K} = (\tilde{q}^2/2) + (\tilde{u}\tilde{v}^3/3) - (b\tilde{v}^2/2)$ is the rescaled version of K. Hence, when $0 < \nu < 1$, there cannot be periodic solutions with $\mathcal{O}(1)$ period of the type studied above.

REMARK 5.2. The case $\nu = 1$ is a generalization of the case $\beta = 1$ studied in Section 6 of [7]. In this case, there is no longer a separation of time scales, since all variables vary at $\mathcal{O}(1)$ rates. In [7], we showed that the boundaries of the existence domain of these singular periodic orbits (labeled as 'disappearance bifurcations' there) occur precisely in this scaling regime.

5.1. The slow manifold $\mathcal{M}$ and the global geometry of its stable and unstable manifolds. The manifold $\mathcal{M}$ is invariant with respect to the full system (5.2) for each $\epsilon \in \mathbb{R}$. Moreover, when $\epsilon = 0$, $\mathcal{M}$ is normally hyperbolic with three-dimensional stable and unstable manifolds that are given by the unions over all u and p on $\mathcal{M}$ of the 1-D manifolds of the saddle points ($\tilde{v} = 0, \tilde{q} = 0$) of the fast subsystems. Hence, by the geometric singular perturbation theory due to Fenichel [12, 21], $\mathcal{M}$ is again normally hyperbolic for $\epsilon > 0$ sufficiently small. Also, the flow on $\mathcal{M}$ is slow, and it is governed by:

$$\tilde{u}' = p, \qquad p' = -a\epsilon^\nu\left(1 - \epsilon^{\rho+\nu}\tilde{u}\right)$$

in the natural slow time scale. Thus, we see that this slow system is in fact 'super' slow, because the evolution of the variables in the slow time is proportional to a

positive power of ϵ. It is also linear, and trajectories on $\mathcal{M}$ are given by branches of hyperbolae:

$$(5.5) \qquad\qquad \Gamma_C: \qquad p^2 = a\epsilon^{-\rho} \left(1 - \epsilon^{\rho+\nu}\tilde{u}\right)^2 + C.$$

Finally, the asymptotes, which are determined by setting by $C = 0$ in (5.5), are precisely the restricted stable and unstable manifolds (lines) ℓ^s and ℓ^u of the saddle fixed point $(\tilde{u}_* = \epsilon^{-(\rho+\nu)}, p = 0)$:

$$(5.6) \qquad\qquad \ell^{s,u}: \qquad p = \pm\sqrt{\frac{a}{\epsilon^\rho}} \left(1 - \epsilon^{\rho+\nu}\tilde{u}\right).$$

The Fenichel theory also implies that the stable and unstable manifolds of $\mathcal{M}$, present when $\epsilon = 0$, persist in the full system (5.2) when $\epsilon > 0$ is sufficiently small, and they are C^r $\mathcal{O}(\epsilon^{1-\nu})$ close to their unperturbed counterparts for all r. Moreover, they consist of the unions over all points on $\mathcal{M}$ of 1-D fast stable and unstable fibers. We denote these persistent manifolds by $W^S(\mathcal{M})$ and $W^U(\mathcal{M})$.

While one branch of the stable manifold coincides with a branch of the unstable manifold when $\epsilon = 0$, the perturbed manifolds $W^S(\mathcal{M})$ and $W^U(\mathcal{M})$ no longer do so. Instead, they intersect each other transversely in two-dimensional intersection surfaces when $0 < \epsilon \ll 1$. These intersections, in which all orbits that are biasymptotic to $\mathcal{M}$ lie, are detected by the adiabatic Melnikov function evaluated along the homoclinic orbits

$$(5.7) \qquad\qquad \tilde{v}_0(t; \tilde{u}_0) = (3b/2\tilde{u}_0)\text{sech}^2(\sqrt{b}t/2), \ \tilde{q}_0 = \dot{\tilde{v}}_0$$

of the unperturbed fast subsystem. The Melnikov function measures the splitting distance between $W^S(\mathcal{M})$ and $W^U(\mathcal{M})$ along a vector in the $\{q = 0\}$ hyperplane normal to the unperturbed homoclinic orbit. Its simple zeroes (and an Implicit Function Theorem argument) imply the existence of transverse intersections of $W^S(\mathcal{M})$ and $W^U(\mathcal{M})$ nearby, see [31]. For the system (5.2), we compute:

$$(5.8) \qquad\qquad \Delta\tilde{K}(\tilde{u}_0, p) = \int_{-\infty}^{\infty} \dot{\tilde{K}}dt = \frac{p}{3}\int_{-\infty}^{\infty} \tilde{v}_0^3 dt.$$

Hence, the simple zeroes occur only on the $\tilde{u}-$axis where $p = 0$. Moreover, by the symmetry in (5.2) that is inherited from (2.4) and given explicitly by a rescaling of (2.6), we see that the manifolds $W^S(\mathcal{M})$ and $W^U(\mathcal{M})$ intersect transversely precisely at $p = 0$ in the $\{q = 0\}$ hyperplane. This calculation is similar to those in [6] and [4].

As stated above, detailed information about these transverse intersections of $W^S(\mathcal{M})$ and $W^U(\mathcal{M})$ is needed in order to prove the existence of the periodic orbits in this regime. In particular, we now focus on the first intersection of $W^s(\mathcal{M})$ and $W^u(\mathcal{M})$ with the hyperplane $\{q = 0\}$, since the fast segments of the singular periodic orbits will lie exponentially close to this first intersection. This intersection is a one-dimensional curve in the two-dimensional manifold $W^s(\mathcal{M}) \cap W^u(\mathcal{M})$. For any point x_0 on this curve, there is an orbit $\Gamma(t; x_0)$ through it, with $\Gamma(0; x_0) = x_0$, that is forward and backward asymptotic to $\mathcal{M}$. Now, the Fenichel theory [12] implies that, for any such $\Gamma(t; x_0)$, there are orbits $\Gamma_{\mathcal{M}}^+(t; x_0^+) \subset \mathcal{M}$ and $\Gamma_{\mathcal{M}}^-(t; x_0^-) \subset \mathcal{M}$ for which $\|\Gamma(t; x_0) - \Gamma^\pm(t; x_0^\pm)\|$ is exponentially small for all $t \geq \mathcal{O}(\frac{1}{\epsilon})$ and $-t \geq \mathcal{O}(\frac{1}{\epsilon})$, respectively. The two points $\Gamma_{\mathcal{M}}^\pm(0; x_0^\pm)$ are the base points of the 1-D fast stable

and unstable fibers on which the point x_0 lies. Here, we have taken advantage of the fact that the forward and backward evolution of the orbit through x_0 may be decomposed geometrically into a component along the stable and unstable fibers and a component given by the (super) slow evolution of the fibers' basepoints. The latter is given precisely by the orbits $\Gamma_{\mathcal{M}}^{\pm}(t; x_0^{\pm})$.

The sets of basepoints on $\mathcal{M}$ of the fast stable and unstable fibers that contain the intersection points x_0 play a central role in the analysis of this section. These sets are given by:

$$(5.9) \quad T_o \equiv \cup_{x_0}\{x_0^- = \Gamma_{\mathcal{M}}^-(0, x_0^-)\} \quad \text{and} \quad T_d \equiv \cup_{x_0}\{x_0^+ = \Gamma_{\mathcal{M}}^+(0, x_0^+)\},$$

where the unions are taken over all $x_0 \in W^S(\mathcal{M}) \cap W^U(\mathcal{M}) \cap \{q = 0\}$. Here, the subscripts o and d denote 'take off' and 'touch down', respectively. Following [6] and [4], the curves T_o and T_d may be obtained explicitly. As we have already seen, $p(t = 0) = 0$ along an orbit that is biasymptotic to $\mathcal{M}$. Then, during the backward and forward semi-infinite fast time intervals $(-\infty, 0)$ and $(0, \infty)$, there are jumps in the p coordinate that are given by

$$\int_{-\infty,0}^{0,\infty} \dot{p}\,dt \sim 3\epsilon^{1-\nu}\frac{b^{3/2}}{\tilde{u}_0},$$

which is $\Delta p/2$. Since the accumulated change in u (which is given by $\Delta u/2$) is of higher order, we get to leading order:

$$(5.10) \qquad\qquad T_{o,d} = \{p = \mp 3\epsilon^{1-\nu}\frac{b\sqrt{b}}{\tilde{u}}\}.$$

In the following subsections, we will separate the analysis of (5.2) into the geometrically distinct cases of $\rho > 0$, $\rho < 0$, and $\rho = 0$, respectively.

5.2. Singular periodic solutions for $\rho > 0$. When $\rho > 0$, the saddle fixed point $(\tilde{u}_* = \epsilon^{-(\rho+\nu)}, p = 0)$ on $\mathcal{M}$ is far away from the origin, since $\nu > 0$ also and hence $\tilde{u}_* \gg 1$. In addition, by (5.6), the lines ℓ^s and ℓ^u are horizontal in a (u,p) coordinate system to leading order:

$$(5.11) \qquad\qquad p \sim \pm\sqrt{a}\epsilon^{-\rho/2}$$

in the regime where $\tilde{u} = \mathcal{O}(1)$, and they have asymptotically large p−intercepts. These aspects of the geometry on $\mathcal{M}$ are sketched in Figure 5.1, as are the take-off and touch-down curves (5.10).

One readily finds that, for each $\tilde{u} = \mathcal{O}(1)$, the line $\tilde{u} = \text{constant}$ (say $\tilde{u}_0$) intersects both T_o and T_d in unique points, as shown. The coordinates of these points are given to leading order by: $(\tilde{u}_0, \mp 3\epsilon^{1-\nu}(b^{3/2}/\tilde{u}_0))$. These two intersection points are the base points of the fast stable and unstable fibers which lie in the transverse intersection of $W^S(\mathcal{M})$ and $W^U(\mathcal{M})$. Moreover, to leading order, they are connected by the homoclinic orbit of the unperturbed fast subsystem with $\tilde{u} = \tilde{u}_0$.

These two intersection points are also connected by a segment of a super slow hyperbolic orbit Γ_C, that may be determined directly from (5.5). This segment is symmetrically disposed about the line $p = 0$, and we calculate:

$$(5.12) \quad C \sim -a\epsilon^{-\rho} + \tilde{C}, \quad \text{where} \quad \tilde{C} = \begin{cases} 2a\epsilon^{\nu}\tilde{u}_0 & \text{if} \quad 0 < \nu < 2/3 \\ 9\epsilon^{2(1-\nu)}\frac{b^3}{\tilde{u}_0^2} & \text{if} \quad 2/3 < \nu < 1 \end{cases}$$
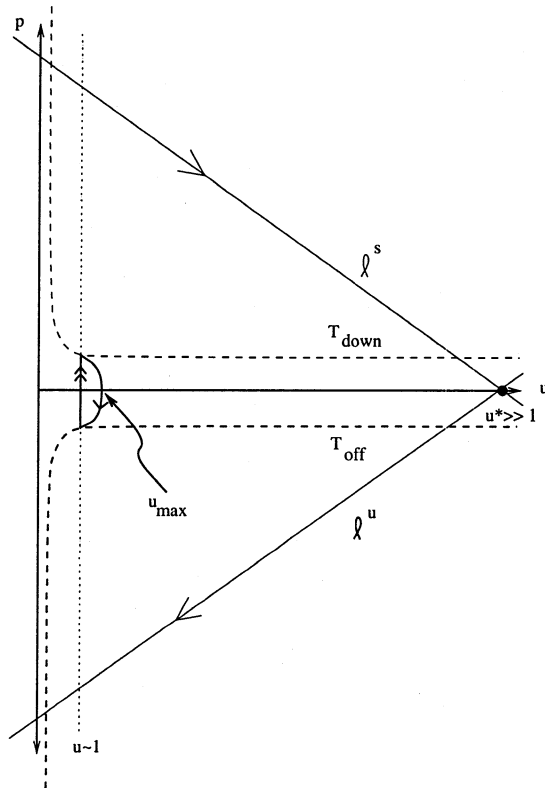
FIG. 5.1. *A sketch of the geometry on the slow manifold $\mathcal{M}$ when $\rho > 0$.*

With this asymptotic information about C in hand, we find the $\tilde{u}$–intercept of the super slow hyperbolic orbit segments, *i.e.*, where they intersect the line $p = 0$. This intercept is the point $(\tilde{u}_{\max}, 0)$, where $\tilde{u}_{\max}$ is the solution of:

$$(5.13) \qquad -2a\epsilon^{\nu}\tilde{u}_{\max} + a\epsilon^{\rho+2\nu}\tilde{u}_{\max}^2 + \tilde{C} = 0.$$

Hence, we find:

$$(5.14) \qquad \tilde{u}_{\max} \sim \begin{cases} \tilde{u}_0 & \text{for} \quad 0 < \nu < 2/3 \\ \epsilon^{2-3\nu}\dfrac{9b^3}{2a\tilde{u}_0^2} & \text{for} \quad 2/3 < \nu < 1. \end{cases}$$

Moreover, we double check that indeed $\tilde{u}_{\max} < \tilde{u}_*$, since $\rho > 0$ here.

The above formal arguments suggest the following Theorem:

THEOREM 5.1. *Let $\rho > 0$, $\beta < (2/3)(\sigma + \alpha)$ and $a, b > 0$, $\mathcal{O}(1)$. For all $u_0 = \epsilon^{\nu}\tilde{u}_0$ with $0 < \nu < 1$ there exists a $v(0; u_0) = \epsilon^{-\nu}\tilde{v}(0; \tilde{u}_0) = \epsilon^{-\nu}\dfrac{3b}{2\tilde{u}_0}$ (to leading order) such that system (2.4) has a singular periodic orbit with initial conditions of the form $(u_0, 0, v(0; u_0), 0)$.*

This result is thus an extension of Theorem 4.1 to the case $0 < u_0 \ll 1$. See Figure 5.2 for a sketch of a family of regular periodic orbits that can be continued via this theorem into the regime in which the periodic orbits are singular. Note that the orbits described in the above Theorem are singular in a number of senses. The
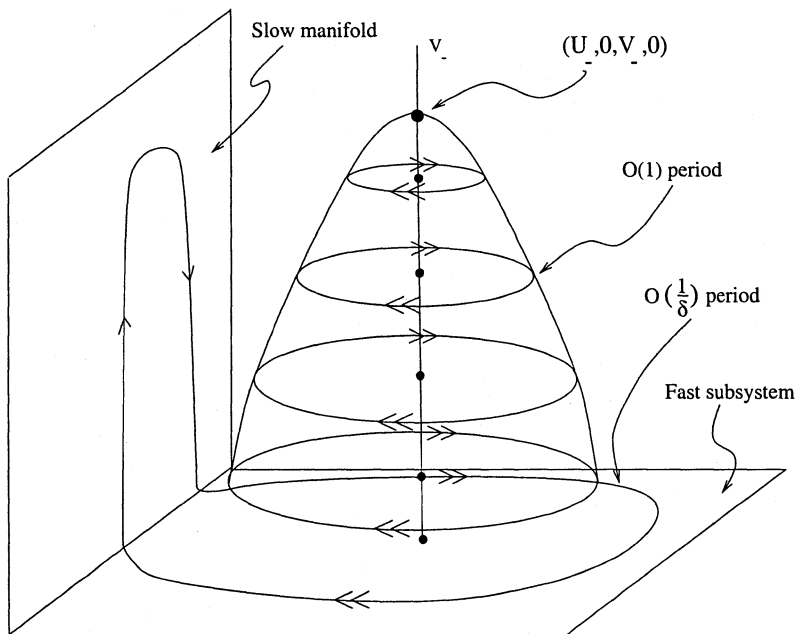
FIG. 5.2. *A sketch of a complete family of periodic orbits of the type whose existence is given by the theorems in Sections 4 and 5 for a fixed a,b pair, when $\rho > 0$.*

v component becomes both exponentially small, since the solution has a component close to $\mathcal{M}$, and asymptotically large $(\mathcal{O}(\epsilon^{-\nu}))$, although this last degeneration is scaled away by the scalings of (5.2). The period is $\mathcal{O}(\epsilon^{-\nu}) \gg 1$, since the solution 'travels' a distance of $\mathcal{O}(\epsilon^{1-\nu})$ ($=$ the distance between T_o and T_d (5.10)) with a speed of $\mathcal{O}(\epsilon) = \dot{p}$ (5.2)) along $\mathcal{M}$. Thus, for the largest part of a period, v is exponentially close to $\mathcal{M}$. This means for $v = V$ as solution of the PDE (1.1) that V is close to $V \equiv 0$ except for periodically spaced sharp 'pulses' (see Figure 5.5). Furthermore, it follows from the above analysis of $\tilde{u}_{\max}$ (5.14) that the solution remains close to the $\{\tilde{u} = \tilde{u}_0\}$ hyperplane as long as $0 < \nu < 2/3$. When $\nu > 2/3$ (but still < 1), the periodic orbit deviates from this hyperplane to $\tilde{u}_{\max} = \mathcal{O}(\epsilon^{2-3\nu}) \gg 1$ (5.14). Note, however, that in the unscaled quantities $u_{\max} = \epsilon^\nu \tilde{u}_{\max} = \mathcal{O}(\epsilon^{3-3\nu})$, thus $u_{\max} \uparrow \mathcal{O}(1)$ only in the singular limit $\nu \to 1$.

Proof. Although the theorem is formulated for solutions of (2.4), it is by construction more convenient to prove the result in terms of solutions to (5.2). Moreover, the method of proof requires that we relocate the initial condition with half a period to the point $(\tilde{u}_{\max}, 0, \tilde{v}_1, 0)$, for which $\tilde{v}_1$ is positive and exponentially small, *i.e.,* a point that lies above and exponentially close to the point $(\tilde{u}_{\max}, 0, 0, 0)$ on $\mathcal{M}$. As t increases, the orbits through these initial conditions stay exponentially close to Γ_C (5.5) until they reach a small neighborhood of the point $(\tilde{u}_0, -3\epsilon^{1-\nu}b^{3/2}/\tilde{u}_0)$ where $\Gamma_C \cap T_o$. Then, from inside a small neighborhood of this point, they 'take off' (*i.e.,* exit any fixed

small neighborhood of $\mathcal{M}$) for a circuit through the fast field, where they are near the homoclinic orbit (5.7) of the fast subsystem. The $\tilde{v}$ component has its maximal value close to the maximum of (5.7). This is the initial condition mentioned in the formulation of the theorem. The orbit through $(\tilde{u}_{\max}, 0, \tilde{v}_1, 0)$ lies exponentially close to the curve along which $W^S(\mathcal{M})$ and $W^U(\mathcal{M})$ intersect transversely during the fast time interval. In addition, during this near-homoclinic excursion their p coordinates make a jump of size Δp, after which they almost 'touch down' on $\mathcal{M}$ near the point $(\tilde{u}_0, 3\epsilon^{1-\nu}b^{3/2}/\tilde{u}_0)$, where $\Gamma_C \cap T_d$, i.e., they approach exponentially close to it, yet remain just above it. After this fast, near-homoclinic excursion, they are exponentially close to Γ_C, with their $\tilde{v}$ and $\tilde{q}$ coordinates exponentially small and decreasing, until they return to their initial conditions $(\tilde{u}_0, 0, \tilde{v}_1, 0)$ completing a periodic orbit.

The rigorous justification of the above geometric arguments is then almost the same as the proof of Theorem 4.2 in [6]. One starts with a one-dimensional segment of initial conditions, namely an interval of points $(\tilde{u}_0, 0, \tilde{v}_1, 0)$ with $\tilde{v}_1$ chosen to lie in a sufficiently large interval of positive, but exponentially small, numbers. Let $\mathcal{L}$ denote the two-dimensional manifold obtained by flowing the initial conditions in this segment forward in time. Then, by tracking $\mathcal{L}$ through the fast and slow regimes using the modified version (see [35]) of the Exchange Lemma with Exponentially Small Error, one can readily show that $\mathcal{L}$ transversely intersects itself in a locally unique curve that contains the desired fast-slow singular periodic orbit, for which the leading order asymptotics are those just described. See the proof of Theorem 4.2 in [6].

REMARK 5.3. This result does not yet give an exact statement on the second boundary of the 1-parameter family of periodic solutions established by Theorems 4.1 and 5.1 (see Remark 4.1). The system (5.2) loses its singular character as $\nu \uparrow 1$, so we cannot consider this limit by the above method. This situation is very similar to the 'disappearance bifurcation' of the homoclinic pulse in the Gray-Scott model considered in Section 6 of [7] that triggers the process of self-replication (see Remark 5.2 and subsection 5.4). There, it has been shown by a topological shooting method that the intersections of $W^S(\mathcal{M})$ and $W^U(\mathcal{M})$ disappear completely as $\epsilon^{1-\nu}$ becomes too large. This method also works for the more general problem of the disappearance of the periodic solutions described by Theorem 5.1. We do not go into the details here. Note that the numerical simulations of [26] suggest that this bifurcation is of a saddle-node type: there is a second singular orbit that does not exist in the case $\nu < 1$.

5.3. Singular periodic solutions for $-\frac{2}{3} < \rho < 0$ and limiting homoclinic solutions. In this subsection, we consider the case $\rho < 0$. Here, the geometry on $\mathcal{M}$ is considerably different from that which we saw in the previous subsection, and it varies with $\nu > 0$. There will be three cases to consider: $\rho + \nu < 0, = 0,$ and > 0.

The location of the saddle-saddle fixed point $(\tilde{u}_*, 0, 0, 0)$ on $\mathcal{M}$ is:

$$(5.15) \qquad \tilde{u}_* = \epsilon^{-(\rho+\nu)} \begin{cases} \ll 1 & \text{if} \quad \rho+\nu < 0 \\ =1 & \text{if} \quad \rho+\nu=0 \\ \gg 1 & \text{if} \quad \rho+\nu>0 \end{cases}$$

By (5.6), the asymptotic behavior of the lines ℓ^u and ℓ^s also depends on which case one is in:

$$(5.16) \qquad p \begin{cases} \sim \mp\sqrt{a}\tilde{u}\epsilon^{(\rho/2)+\nu} & \text{if} \quad \rho+\nu < 0 \\ =\pm\sqrt{a}\epsilon^{-\rho/2}(1-\tilde{u}) & \text{if} \quad \rho+\nu=0 \\ \sim\pm\sqrt{a}\epsilon^{-\rho/2} & \text{if} \quad \rho+\nu>0. \end{cases}$$
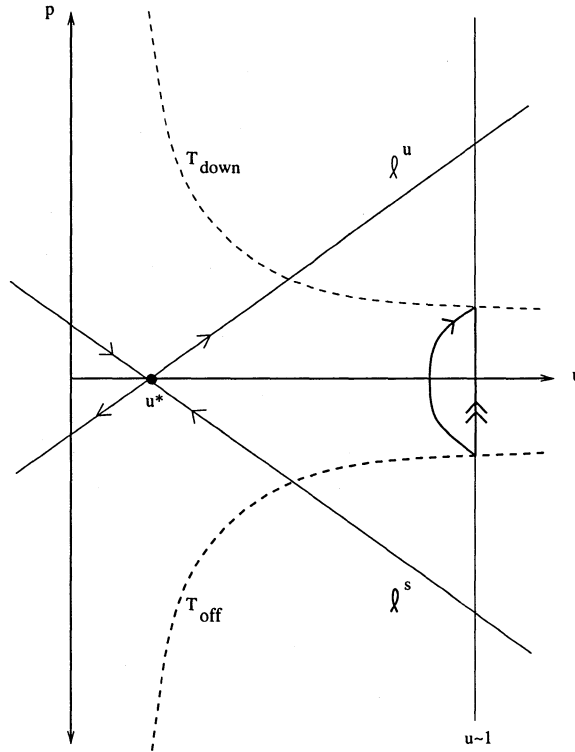
FIG. 5.3. *A sketch of the geometry on the slow manifold* $\mathcal{M}$ *when* $-2/3 < \rho < 0$ *and* $\rho + \nu < 0$.

We note for completeness that the curves T_o and T_d are here also given by (5.10), since they are independent of ρ to leading order.

Since we assume $\rho < 0$ and we consider ν as a parameter that is increased from 0 to 1 (*i.e.*, the magnitude of $u_0 = \mathcal{O}(\epsilon^\nu)$ decreases), we first consider the case $\rho + \nu < 0$. The geometry on $\mathcal{M}$ for $\rho + \nu < 0$ is illustrated in Figure 5.3. This figure reveals that singular periodic orbits of the type found in subsection 5.2 do not exist here. The lines of constant $\tilde{u}$ with $\tilde{u} = \mathcal{O}(1)$ intersect ℓ^s and ℓ^u above $\tilde{u}_*$, since $\tilde{u}_* \ll 1$. Moreover, in the subcase $1 - \nu \geq (\rho/2) + \nu$, the horizontal distance between T_o and T_d is less than (or asymptotically equal to) that between ℓ^s and ℓ^u, as shown in Figure 5.3. Hence, the relevant super slow hyperbolic orbit segment Γ_C on $\mathcal{M}$ flows from left to right, which is the same direction in which p changes/jumps during the near-homoclinic excursion in the fast field. Therefore, these fast and slow orbit segments cannot be hooked up to form a singular periodic orbit. In the complementary subcase $1 - \nu < (\rho/2) + \nu$, the curves T_o and T_d lie outside of the lines ℓ^s and ℓ^u for $\tilde{u} = \mathcal{O}(1)$. Hence, here also, it is not possible to find singular periodic orbits.

The root of the problem in the case just considered is that $\tilde{u}_* \ll 1$, so that lines of constant $\mathcal{O}(1)$ $\tilde{u}$ intersect the lines ℓ^s and ℓ^u above $\tilde{u}_*$. We now turn to consider the second and third cases $\rho + \nu \geq 0$, in which the horizontal lines of constant and $\mathcal{O}(1)$ $\tilde{u}$ with $\tilde{u} < 1$ can intersect ℓ^s and ℓ^u below $\tilde{u}_*$, since $\tilde{u}_* \geq \mathcal{O}(1)$. So, here there is hope to find singular periodic orbits similar to those found in subsection 5.2. The key ingredient is to find $\mathcal{O}(1)$ values of $\tilde{u}$ such that the horizontal distance between

T_o and T_d is less than that between ℓ^s and ℓ^u. Let us denote these distances by $\Delta T_{od}(\tilde{u})$ and $\Delta \ell^{su}(\tilde{u})$, respectively. Then, by (5.10) and (5.16), the requirement that $\Delta T_{od}(\tilde{u}) \leq \Delta \ell^{su}(\tilde{u})$ implies

$$(5.17) \qquad\qquad 1 - \nu \geq -\frac{\rho}{2}.$$

Hence, in the second case, when $\rho + \nu = 0$, we see directly that we must impose the following restriction:

$$(5.18) \qquad\qquad -\frac{2}{3} \leq \rho < 0.$$

In the third case, when $\rho + \nu > 0$, the jump condition (5.17) implies that attention must be restricted to $-\rho < \nu \leq (\rho/2) + 1 \subset (0,1)$ (and hence also $-2/3 < \rho < 0$). Note that this ν region for existence shrinks to $\nu = 2/3$ as $\rho \to -2/3$. Setting aside the boundary case of $\rho = -2/3$ for subsection 5.4 below, we are now in a position to establish, in terms of the scalings of Section 2 and here:

THEOREM 5.2. *Let* $-\frac{2}{3} < \rho < 0$, $\beta < (2/3)(\sigma + \alpha)$ *and* $a, b > 0$, $\mathcal{O}(1)$. *There exist* $\tilde{u}_{hom}^1, \tilde{u}_{hom}^2 > 0$ *such that for all*

$$u_0 \in (\tilde{u}_{hom}^2 \epsilon^{1+(\rho/2)}, \tilde{u}_{hom}^1 \epsilon^{-\rho})$$

there exists a singular periodic orbit of (2.4). Moreover, for

$$u_0 = \tilde{u}_{hom}^1 \epsilon^{-\rho} \quad \text{and} \quad u_0 = \tilde{u}_{hom}^2 \epsilon^{1+(\rho/2)},$$

to leading order, there exists a singular orbit homoclinic to the fixed point $(\epsilon^\rho, 0, 0, 0) \in \mathcal{M}$.

See Figure 5.4 for an illustration. Thus, in this case, we do have explicit descriptions of both boundaries of the u_0 region in which existence has been shown. Both of these boundaries correspond to a singular one-pulse solution of (1.1) that is biasymptotic to the trivial pattern ($U = 1, V = 0$). Note that this theorem is an extension to the case $\rho = 2\beta - \alpha < 0$ of the $4b^2 > a$ case of Theorem 4.3 here.

Proof. The proof of the existence of the periodic orbits is completely similar to that of Theorem 5.1 (and thus to that of Theorem 4.2 in [6]) as soon as we know that there is, for a given $\nu \in (0,1)$, an intersection of $T_{o,d}$ with a line $\tilde{u} = \tilde{u}_0$ ($\tilde{u}_0 = \mathcal{O}(1)$) inside the triangle bounded by $\ell^{s,u}$, below $\tilde{u} = \tilde{u}_*$. Then, one can formally construct a singular periodic orbit in (5.2) that consists of two parts. There is a fast excursion outside $\mathcal{M}$ near the homoclinic orbit (5.7) by which the orbit can jump from T_o to T_d. The two intersection points $T_{o,d} \cap \{\tilde{u} = \tilde{u}_0\}$ can also be connected by (super slow) hyperbolic orbit segment Γ_C on $\mathcal{M}$ (5.5). This singular geometric construction can again be justified by the Exchange Lemma for periodic orbits [35].

The two limiting homoclinic orbits mentioned in the theorem, that can be seen as singular periodic orbits with (spatial) period $\to \infty$, determine the critical values ($\nu = -\rho, \tilde{u}_0 = \tilde{u}_{hom}^1$) and ($\nu = 1 + \rho/2, \tilde{u}_0 = \tilde{u}_{hom}^2$) for which these intersections exist (see Figure 5.4). For $\nu = -\rho$ we have $\tilde{u}_* = 1$, thus the $\tilde{u}$ component $\tilde{u}_{hom}^1 < 1$ (by definition) of the intersections $\ell^{s,u} \cap T_{o,d}$ is of $\mathcal{O}(1)$. These intersections correspond by construction to an orbit in $W^S(\mathcal{M}) \cap W^U(\mathcal{M})$ that is biasymptotic to $(\tilde{u}_*, 0, 0, 0) \in \mathcal{M}$. Note that the $\tilde{u}$-component of this homoclinic orbit is always $\mathcal{O}(\epsilon^{1+\rho})$ close to 1 (therefore one does not expect this orbit to be stable).

As one decreases ν, the distance $\Delta T_{od}(\tilde{u})$ between $T_{o,d}$ increases. By (5.17), there is a critical value, $\nu = 1 + \rho/2$, at which $\Delta T_{od}(\tilde{u}) \sim \Delta \ell^{su}(\tilde{u})$ for $\tilde{u} = \mathcal{O}(1)$. Thus, there are again intersections $\ell^{s,u} \cap T_{o,d}$ with an $\tilde{u}$-component $\tilde{u}_{hom}^2$ (by definition) of $\mathcal{O}(1)$, and these directly yield the second homoclinic orbit to $(\tilde{u}_*, 0, 0, 0)$ in $W^S(\mathcal{M}) \cap W^U(\mathcal{M})$.

REMARK 5.4. The second limiting case, $\nu = 1 + \rho/2$, gives an explicit relation between the scaled ODEs studied in [6], [7], [4] and the ODEs studied in this paper. In [6], [7], [4] the existence and stability of singular homoclinic solutions (and some singular periodic patterns) to (1.1) has been studied. The existence has been obtained in an ODE with rather special scaling. This ODE is recovered in the context of this paper by setting $\nu = 1 + \rho/2$ in (5.2). In a sense this is natural, since the derivation of the scaling in [6] is based on the 'jump condition' $\Delta T_{od}(\tilde{u}) \sim \Delta \ell^{su}(\tilde{u})$. The crucial parameter $\epsilon^{1-\nu}$ of (5.2) now becomes $\delta^{\alpha/2-\beta} = \sqrt{A}/B$ (see (2.3)). The dissappeance or splitting bifurcation studied in [7], [4] occurs as $\rho = 0$ or $\alpha/2 - \beta = 0$, i.e. $A \sim B^2$ [4] (or in [7] where only $A = \mathcal{O}(\delta^2)$ was considered: $\beta = 1$).

5.4. Remarks on outstanding cases.

The case $\rho = -2/3$. First, we note by (2.5) that $\rho = -2/3$ corresponds to $\beta = \frac{1}{3}(\alpha - 2\sigma)$, i.e. it determines the line ℓ_{hom} in the (α, β)-parameter space (see the Introduction). It follows from the above analysis that there can only be (singular) periodic solutions for $\nu = 2/3$, i.e. $u_0 = \mathcal{O}(\epsilon^{2/3})$ in (2.4). This situation is completely analogous to the special case $\alpha = 0$ considered in section 4.3 of [6]. In this case both homoclinic bifurcations described by Theorem 5.2 appear in the same scaling, again defined by the intersections $\ell^{s,u} \cap T_{o,d}$ and labeled by $\tilde{u}_{hom}^{1,2}$. As long as the parameters a and b are such that $\ell^{s,u} \cap T_{o,d} \neq \emptyset$ there is a 1-parameter family of singular periodic orbit bounded by homoclinic orbits (as in Theorem 5.2). However, it is a straightforward exercise to show that the intersections $\ell^{s,u} \cap T_{o,d}$ disappear as $a > 144b^3$ (to leading order); i.e., $\tilde{u}_{hom}^{1,2}$ merge as $a = 144b^3$ (to leading order), where there is a saddle node bifurcation of homoclinic orbits (see [6] for more details).

The case $\rho < -2/3$. This case can be considered as the continuation of the above case to $a \gg 1$ (2.3): it follows immediately that there are no periodic or homoclinic orbits, because $\Delta T_{od} \gg \Delta \ell^{su}$ for $\mathcal{O}(1)$ values of $\tilde{u}$.

The case $\rho = 0$. The regular periodic orbits have already been considered in Theorem 4.3. Their continuation is completely analogous to that of the case $\rho < 0$ in Theorems 5.1 and 5.2 as long as $0 < \nu < 1$. The bifurcation as $\nu \to 1$ can be seen as a combination of the 'disappearance' bifurcation discussed in Remarks 5.3 and the homoclinic bifurcation at $u_0 = \tilde{u}_{hom}^2 \epsilon^{1+\rho/2}$ $(= \mathcal{O}(\epsilon)$ for $\rho = 0)$ described by Theorem 5.2 (see also Remark 5.4). The case $\rho = 0$ corresponds to the 'splitting bifurcation' that is the onset of the self-replication process [7], [4]. The details of this bifurcation are still not fully understood, and we do not consider it in any more detail in this paper.

The second (or first) homoclinic bifurcation at $u_0 = \tilde{u}_{hom}^1 \epsilon^{-\rho}$ described by Theorem 5.2 for $\rho < 0$ cannot be extended immediately since for $\rho = 0$ $u_0 = \tilde{u}_{hom}^1 \epsilon^{-\rho} = \mathcal{O}(1)$, i.e. one cannot use (5.2). On the other hand, we note that (2.4) and (5.2) are identical in the case $\nu = \rho = 0$. Thus, we can apply the arguments in the proof of Theorem 5.2 by which the existence of the homoclinic orbit associated to $\tilde{u}_{hom}^1$ is established directly to (2.4). It follows that there is an orbit in $W^S(\mathcal{M}) \cap W^U(\mathcal{M})$ that
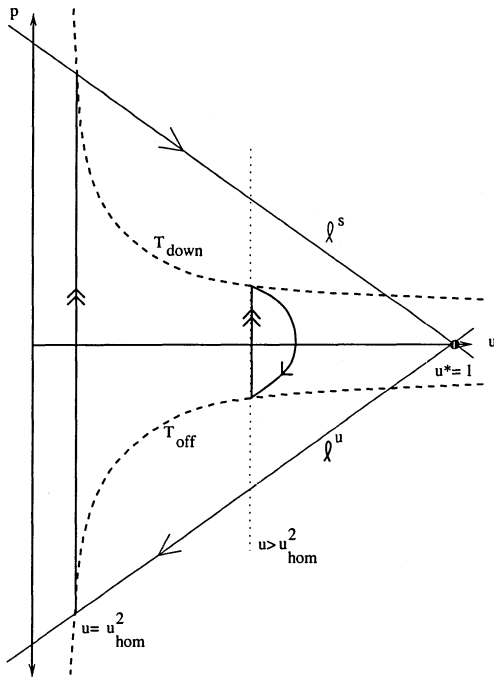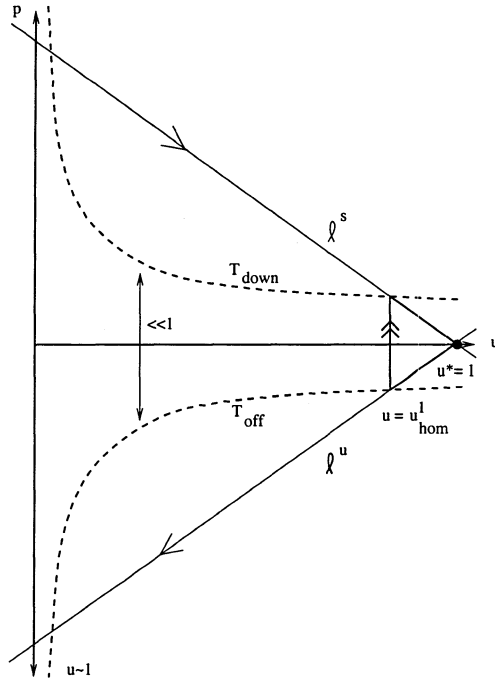
FIG. 5.4. *A sketch of the geometry on the slow manifold* $\mathcal{M}$ *when* $\rho < 0$ *and* $\rho + \nu \geq 0$. *showing the singular periodic orbits in frame b, and the limiting homoclinic orbits at* $u = u_{hom}^1$ *in frame a, and at* $u = u_{hom}^2$ *in frame b.*
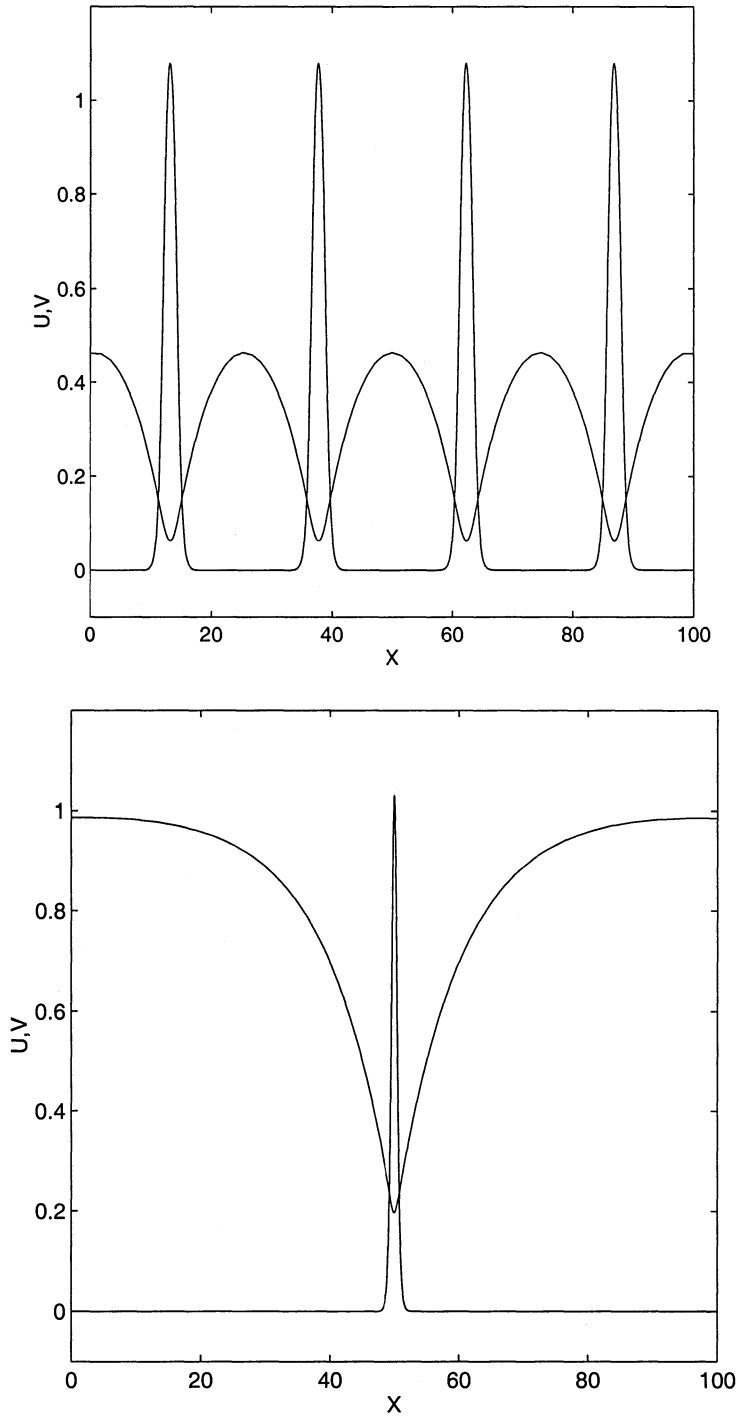
FIG. 5.5. **a.** *A singular periodic solution of (1.1) for* $A = 0.01, b = 0.060, D_u = 1, D_v = 0.01.$
b. *A singular one-pulse homoclinic solution of (1.1) with u given by* u_{hom}^2 *for* $A = 0.01, B = 0.142,$
$D_u = 1, D_v = 0.01.$

is biasymptotic to $(1, 0, 0, 0) \in \mathcal{M}$ with a u-component that is almost 1 everywhere along the orbit. Thus, this is a regular homoclinic orbit in the sense that it forms the boundary at $u_0 = 1$ of the region of regular periodic orbits described by Theorem 4.3.

The case $\beta = (2/3)(\alpha + \sigma)$ with a not close to a_c. This case is not related to the geometric analysis in this section: it forms the continuation of the analysis of Section 3 (where $\beta = (2/3)(\alpha + \sigma)$) to that of Sections 4 and 5 whereas we imposed $\beta < (2/3)(\alpha + \sigma)$ in all theorems. This was necessary since we needed to be able to consider $\epsilon = \delta^{-(3/2)(\beta - 2/3(\alpha + \sigma))}$ as an asymptotically small parameter. The connection between these two cases can be made by starting with a close to, but smaller than, a_c (3.6), and decrease a towards $0 < a \ll 1$. However, as long as $a = \mathcal{O}(1)$ neither the local analysis of Section 3 nor the asymptotic analysis of Sections 4 and 5 can be applied.

We do not intend to consider this case in any detail in this paper (see also below). Still, a combination of the results of Sections 3, 4 and 5 indicates that something interesting must happen in this region. When $a \approx a_c$, there is a 1-parameter band of periodic solutions that limits on the critical point $(u_-, 0, v_-, 0)$ (or the trivial state $(U \equiv U_-, V \equiv V_-)$) at both boundaries of its interval of existence (see Theorem 3.2: the boundaries correspond to the limits $R \to 0$ and $\kappa \to \pm 1/(2b)^{1/4}$ (3.28)). When $a \ll 1$ we have $\beta < (2/3)(\alpha + \sigma)$, so the results of Sections 4 and 5 can be applied. Assuming that we started with $\rho > 0$ (as we did in Section 3) we know that still $\rho > 0$ as β has become less than $(2/3)(\alpha + \sigma)$. Thus Theorem 4.1 yields the existence of a 1-parameter family of periodic orbits. By Remark 4.1 we know that one boundary of the region of existence is still given by the critical point $(u_-, 0, v_-, 0)$ or trivial state $(U \equiv U_-, V \equiv V_-)$. However, the other boundary is now of a totally different nature. As u_0 becomes $\ll 1$ the regular orbits become singular (Theorem 5.1) and the 'boundary' at $u_0 = \mathcal{O}(\epsilon)$ is now given by the 'splitting or disappearance bifurcation' (Remark 5.3).

Thus, we are led to conclude that there is a bifurcation value $a = a_* < a_c$ for $\beta = (2/3)(\alpha + \sigma)$ at which the band of periodic orbits detaches at one side from the critical point $(u_-, 0, v_-, 0)$. The arguments of Remark 5.3 suggest that after this bifurcation the new boundary of the interval of periodic solutions is formed by a saddle node bifurcation at which the periodic solution now 'disappears'.

In Section 6 we shall see that this phenomenon is not at all important in practice/numerical simulations, since the only stable orbits are those that remain quite close to $(U \equiv U_-, V \equiv V_-)$. Hence, the orbits close to this new (conjectured) saddle node bifurcation are not stable. However, understanding this saddle node bifurcation in the case $\beta = (2/3)(\alpha + \sigma)$ might shed some light on the still not completely understood process of self-replication in the Gray-Scott model (Remark 5.3, 5.4, [4, 6, 7, 23, 24, 25, 26, 27, 28, 29, 30]).

6. Numerical simulations. In this section, we compare the results of numerical simulations with quantities used in the existence analysis in order to corroborate this analysis, and we numerically extend the stability results of Section 3 beyond the regime $0 < |A - A_c| \ll 1$ to all $A < A_c$, where we recall that $A_c = a_c \delta^\alpha = \sqrt{g} b^{3/2} \delta^{3\beta/2 + \sigma}$ by (3.6) and the scalings (2.3) of Section 2. We use the code described in [2], [6], [38] to simulate (1.1) with both Dirichlet and Neumann boundary conditions.

6.1. Numerical simulations complementing the existence analysis. In this subsection, we compare the results from numerical simulations with the analytical existence results of Section 3. Specifically, we focus on the integral Δp, (4.2), and

then show that to leading order, $\Delta p = 0$. For this subsection only, we reintroduce hats on the appropriate variables.

The numerical simulations were run using boundary conditions of Dirichlet type. The initial data used were large-amplitude, localized perturbations of the homogeneous state $(U, V) = (1, 0)$. The simulations were run until the resulting pattern stabilized, and the resulting solutions were used to compute values in the expressions below.

Before we can analyze $\Delta p = 0$ numerically, it is necessary to rewrite the expression for Δp using the unscaled variables u and v. Using (4.2) and recalling that $\epsilon \equiv \delta^{\sigma - 3\beta/2 + \alpha}$, we first write the leading order integral as:

$$(6.1) \qquad \Delta p(K_0, \hat{u}_0, p_0) \sim 2T_\epsilon \delta^{\sigma - \frac{3}{2}\beta + \alpha} \left(\left[\frac{\hat{u}_0}{T_\epsilon} \int_{-T_\epsilon}^0 \hat{v}^2 dt \right] - a \right).$$

Rewriting this in terms of the unscaled u_0 and v (recall (2.3)), we then obtain

$$(6.2) \qquad \Delta p \sim \delta^{\sigma - \frac{3}{2}\beta} \left[2T_\epsilon u_0 <v^2> -2T_\epsilon \delta^\alpha a \right],$$

where

$$(6.3) \qquad <v^2> \equiv \frac{1}{T_\epsilon^x} \int_{-T_\epsilon^x}^0 v^2 dx = \frac{1}{T_\epsilon} \int_{-T_\epsilon}^0 v^2 dt = \frac{1}{T_\epsilon^{\tilde{x}}} \int_{-T_\epsilon^{\tilde{x}}}^0 v^2 d\tilde{x}.$$

T_ϵ^x is the period of a periodic orbit with respect to the independent variable x of (2.1), and $\tilde{x}$ is the scale used in numerical simulations ($\tilde{x} = 10^{-2} x$).

In order to analyze the result $\Delta p = 0$ numerically, we will express both terms in square brackets in (6.2) using the quantities computed numerically from the simulations. Using data from the simulations, we found $T_\epsilon^{\tilde{x}}$ and u_0, and computed the integral

$$(6.4) \qquad <v^2> = \frac{1}{T_\epsilon^{\tilde{x}}} \int_{-T_\epsilon^{\tilde{x}}}^0 v^2 d\tilde{x}.$$

Also, $T_\epsilon^{\tilde{x}}$ can be rescaled in terms of T_ϵ by using the scaling of the independent variable x in (2.3), yielding the conversion factor:

$$(6.5) \qquad T_\epsilon = 10^2 \delta^{-\sigma + \frac{\beta}{2}} T_\epsilon^{\tilde{x}}.$$

We can now rewrite the two terms in (6.2). We work on each term separately, beginning with the first term. Using (6.3) and (6.5), we have

$$(6.6) \quad 2T_\epsilon u_0 <v^2> = \frac{2T_\epsilon u_0}{T_\epsilon^{\tilde{x}}} \int_{-T_\epsilon^{\tilde{x}}}^0 v^2(\tilde{x}) d\tilde{x} = \left(2u_0 \int_{-T_\epsilon^{\tilde{x}}}^0 v^2(\tilde{x}) d\tilde{x} \right) 10^2 \delta^{-\sigma + \frac{\beta}{2}}.$$

We obtain a numerical estimate of the term in parentheses using data obtained from the numerical simulations. Similarly, for the second term in brackets in (6.2) we have

$$(6.7) \qquad 2T_\epsilon \delta^\alpha a = 2 \times 10^2 \delta^{-\sigma + \frac{\beta}{2}} T_\epsilon^{\tilde{x}} \delta^\alpha a.$$

Finally, we see that upon equating the right-hand sides of (6.6) and (6.7), it must be that the data from our numerical simulations satisfies:

$$(6.8) \qquad 2u_0 \int_{-T_\epsilon^{\tilde{x}}}^{0} v^2(\tilde{x})d\tilde{x} = 2T_\epsilon^{\tilde{x}} \delta^\alpha a,$$

in order for $\Delta p = 0$ to leading order. The following table presents the results for both sides of this equality, as calculated from simulations using the indicated parameter values (with $\alpha = 1, \beta = 2/3, \sigma = 1$, so that $\rho = 1/3$):

a	b	δ	$2 \int_{-T_\epsilon^{\tilde{x}}}^{0} u_0 v^2(\tilde{x})d\tilde{x}$	$2T_\epsilon^{\tilde{x}} \delta a$
6	0.37	0.13	0.0029	0.0033
9	0.37	0.1	0.0030	0.0032
9	0.4	0.1	0.0031	0.0034
10	0.42	0.09	0.0032	0.0035

Note that the rightmost two columns of the table, which represent only the leading order terms of Δp, are in close agreement. The next order term in the asymptotic expansion for Δp is of order $\epsilon^{1+\rho}$. Thus, the relative error (ϵ^ρ) is $\delta^{1/3}$, since $\rho = 1/3$ and $\alpha - 3\beta/2 + \sigma = 1$. Hence, we have that numerically, $\Delta p = 0$ to leading order. This agrees well with the analytical results of Section 3.

6.2. Busse balloon. In [3], a nonlinear stability analysis of the stationary roll cell pattern in the Rayleigh-Benard convection is presented. The stability with respect to infinitesimal perturbations is determined analytically from the eigenvalue problem for the most unstable mode, where this eigenvalue problem is derived via an orthogonality condition, similar in spirit to what was done here in Section 3 and Appendix A. In addition, a fully nonlinear stability analysis, carried out numerically, reveals that there is a 'balloon' in the three-dimensional (Rayleigh number, Prandtl number, and norm of the wave number vector) parameter space in which they are stable. For each value of the Prandtl number within a given range, the cross- section in the Rayleigh number-wave vector plane of the balloon is a closed region. Here, we will find a similar result in the three-dimensional parameter space B, A, k, respectively.

For each fixed pair of $\mathcal{O}(1)$ parameters a and b, we have shown that (1.1) has multiple stationary, spatially-periodic solutions. In Section 3 we also analytically showed the stability of a subset of these solutions, for a close to the critical a_c. In this section, we determine bounds on the wave number k for which these stable periodic states are found in simulations of the full PDE. As stated above, the results may be characterized as a Busse balloon (see Figure 6.1), and can be viewed as a numerical extension of the analytical stability results of Section 3 to include a values well below a_c. For this section, we will consider the unscaled versions A and B of a and b.

To illustrate the numerical extension, we thoroughly document the case $B = 0.086$ ($b = 0.4, \beta = 2/3$ and $\sigma = 1$) and $\delta = 0.1$. The upper tip of the balloon was found numerically to lie near $A = 0.115$ and $k = 1.9$. By contrast, the analysis in Section 3 yields $A_c = 0.104$ and $k_c(A) = 1.89$ to leading order. Moreover, in Appendix B, we calculate the next order term in the asymptotic expansion of A_c. We therefore have:

$$(6.9) \qquad A_c \sim \sqrt{g}b^{3/2}\left(1 + \delta^{2\beta-\alpha}\sqrt{b}\left[\frac{3 + 2\sqrt{2}}{2}\right]\right).$$

Hence, for $b = 0.4$ and $\delta = 0.1$, with $\alpha = 0$ and $\beta = 2/3$, we get: $A_c \approx 0.1138$, which agrees extremely well with the data from the numerical simulations.
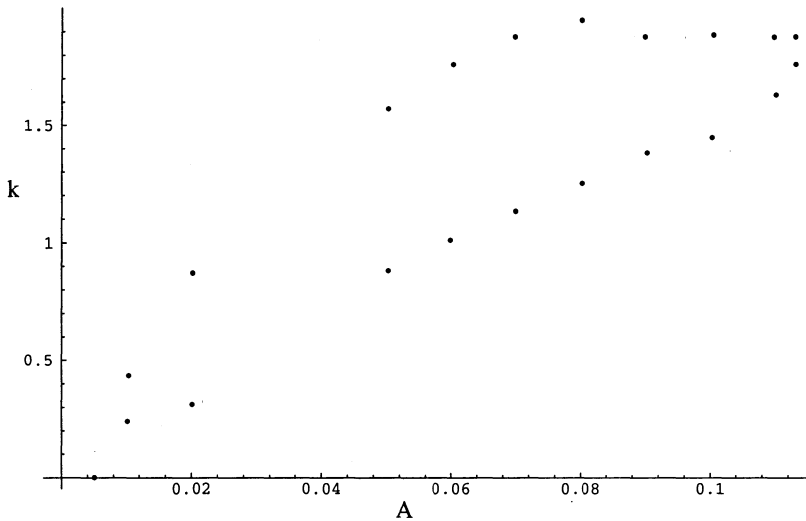
FIG. 6.1. *Data from numerical simulations plotted in the $A - k$ plane indicating the boundary of the region of stable stationary, spatially periodic solutions of (1.1), i.e., of the Busse balloon, for $D_U = 1.0$, $D_V = 0.01$, and $B = 0.086$ ($\delta = 0.1$, $\sigma = 1$). Note that only k corresponding to integer or half-integer numbers of pulses on the domain were counted, hence the actual boundary is smoother, and also the data near the upper tip of this Busse balloon may be compared to the stability parabola shown in Figure 3.2.*

For a sequence of fixed A values below this critical A value, namely for

$$A \in \{0.02, 0.05, 0.06, 0.07, 0.08, 0.09, 0.1, 0.11, 0.111, 0.112, 0.113, 0.114, 0.115, 0.116\},$$
(6.10)

we find intervals of k values corresponding to the wave numbers of stable periodic solutions. The results are shown in Figure 6.1, and the method used to obtain these results is described in the following three paragraphs.

The initial data used was

$$(6.11) \qquad \begin{pmatrix} U \\ V \end{pmatrix} = \begin{pmatrix} U_- \\ V_- \end{pmatrix} + \begin{pmatrix} c_1 U_- \cos(2\pi n x) \\ c_2 V_- \cos(2\pi n x) \end{pmatrix}$$

where (U_-, V_-) is the stationary pattern corresponding to the chosen parameters (A, B), $0 < c_1 < 1, 0 < c_2 < 1$ are amplitude scaling parameters (and we remark that here c_1 and c_2 are different variables from those used in subsection 3.2). Specifically, for each fixed n, this initial data has n spikes on a unit interval. With a, b and δ fixed, we conducted simulations with a range of values of n in order to be sure that we sampled the basins of attraction of all of the stable periodic states. (It was not always the case however, that N-spike initial data on $[0, 1]$ corresponded to an N-spike solution.)

The simulations were run with Neumann boundary conditions, and they were run long enough in order for the pattern to stabilize. A value for k was then calculated by determining the wavelength of the (periodic) pattern, and computing $k = \frac{2\pi}{\lambda}$. This process was repeated for each n, and terminated in the following way. For each fixed A and B, the parameter n was increased (decreased) and simulations run until an n was obtained such that the resulting pattern was either no longer periodic, or else

was periodic, but with a k-value less than (greater than) the previous simulation (corresponding to the stable pattern having a larger (smaller) characteristic wavelength than the previous simulation), respectively. For example, for $A = 0.1$, when $n = 20$, the resulting stable periodic pattern obtained has a corresponding k-value of 1.91, and for $n = 21$ the k-value is 1.97, while for $n = 22$, the k-value is found to be 1.70. Thus, we deduce that the largest wave number for which a stable stationary pattern exists is $k = 1.97$ for $A = 0.1$.

For $A = \{0.05, 0.1, 0.112, 0.113, 0.114\}$, the simulations near the boundary of the Busse balloon were run until at least $T_{end} = 20,000$, in order to insure that the patterns found were stable. In this way, and with the restriction that we only find solutions with integral or half-integral numbers of pulses, we obtained the location of the boundary with reasonable accuracy, at least for A sufficiently large.

Numerically, we find that the lower tip of the Busse balloon lies near $A = 0.0054$. At this point, the singular homoclinic orbit given by $\tilde{u}^2_{hom}$ in Theorem 5.2 (see Figure 5.5) undergoes a Hopf bifurcation. In this range of parameters it is possible to apply the stability theory for singular patterns developed in [7, 8]. In the scaling, namely $A = \mathcal{O}(\delta^2)$ and $\sigma = 1$, assumed throughout those papers, the theoretical (and rigorous) stability boundary is to leading order $b_{\text{Hopf}}(a) = (0.66)\sqrt{a}$ when $\beta = 1/2$, or, in unscaled quantities: $B_{\text{Hopf}}(A) = (0.66)\sqrt{A/\delta}$. It is shown in [4] that this last version also holds for more general scalings of A and B. Moreover, we can introduce σ and rewrite the Hopf bifurcation curve in (A, B)-parameter space as (see [4]):

$$(6.12) \qquad A_{\text{Hopf}}(B) = \frac{B^2}{0.66^2}\delta^\sigma$$

Thus, it follows that here A_{Hopf} should be ≈ 0.0017. The error is well within the theoretical boundaries. The asymptotic theory yields that the leading order correction to the number ≈ 0.66 in (6.12) is of the order $\mathcal{O}(\sqrt{A}/B)$, [7, 4]. Here we find that one has to replace ≈ 0.66 by ≈ 0.37 in (6.12) to find $A_{\text{Hopf}} = 0.0054$, while $\sqrt{A}/B \approx 0.85$ (note that this is not really an asymptotically small quantity!).

Finally, we close this discussion on the Busse balloon by referring to the results on the stability of singular periodic orbits as described by Theorem 5.2 for $u_0 = \mathcal{O}(\epsilon^{1+(\rho/2)})$ in [7, 8, 4] (see also Remark 5.4). It has been shown in [7] that for $A > A_{\text{Hopf}}$ there is a band of stable singular patterns, see Figure 5.5. One of the boundaries of this band is formed by the homoclinic pattern. Thus, the theory of Ginzburg-Landau equations gives an analytical theory for the existence of the Eckhaus band of stable solutions [9, 34] at the upper tip of the Busse balloon, while the work in [7, 8] gives analytical results on the 'singular Eckhaus band' of stable solutions near the lower tip of the Busse balloon.

A. Derivation of the Ginzburg-Landau equation. In this appendix, we outline the steps in the derivation of the Ginzburg-Landau equation used in the stability analysis of Section 3. We refer to [9] and the references therein for more background.

In order to derive the Ginzburg-Landau equation, we extend the expansion (3.26) in powers of γ and Fourier modes:

$$\begin{pmatrix} U \\ V \end{pmatrix} = \mathcal{A}(\xi, \tau) \begin{pmatrix} 2 \\ -\frac{1}{2}(1 + g) \end{pmatrix} e^{ik_c x} + \gamma \begin{pmatrix} X_{12}(\xi, \tau) \\ Y_{12}(\xi, \tau) \end{pmatrix} e^{ik_c x} + \gamma \begin{pmatrix} X_{02}(\xi, \tau) \\ Y_{02}(\xi, \tau) \end{pmatrix} + \cdots$$

$$+\gamma^2 \left(\begin{array}{c} X_{22}(\xi,\tau) \\ Y_{22}(\xi,\tau) \end{array} \right) e^{ik_c x} + \text{c.c.} + \cdots$$

$$\text{(A.1)} \qquad \gamma \left(\begin{array}{c} X_{13}(\xi,\tau) \\ Y_{13}(\xi,\tau) \end{array} \right) e^{2ik_c x} + \text{c.c.} + \cdots$$

By substituting this expansion into (3.22) and collecting like powers of γ and $e^{ik_c x}$, we can solve for the unknowns $X_{02,12,22,13,...}$ and $Y_{02,12,22,13,...}$ in succession. We first note that, after plugging in the expansion, the right-hand side of (3.22) is of $\mathcal{O}(\gamma^2)$. Thus, only the equation for $(X_{13}, Y_{13})^T$ involves the right-hand side of (3.22). The equation for $(X_{02}, Y_{02})^T$ is

$$\text{(A.2)} \qquad \left(\begin{array}{c} X_{02} \\ Y_{02} \end{array} \right) = 4|\mathcal{A}|^2 \sqrt{\frac{g}{b}} \left(\begin{array}{c} 1 \\ 0 \end{array} \right).$$

The equation for (X_{22}, Y_{22}) is

$$\text{(A.3)} \qquad \left(\begin{array}{c} X_{22} \\ Y_{22} \end{array} \right) = \frac{2}{9}\mathcal{A}^2 \sqrt{\frac{g}{b}} \left(\begin{array}{c} 3 - 2g \\ 2g - 2 \end{array} \right).$$

For $(X_{1j}, Y_{1j})^T$, we find equations of the form

$$\text{(A.4)} \qquad b\mathcal{M}_c \left(\begin{array}{c} X_{1j} \\ Y_{1j} \end{array} \right) = \left(\begin{array}{c} I_1 \\ I_2 \end{array} \right),$$

where $\mathcal{M}_c$ is as defined in (3.24). Note that for $(X_{12}, Y_{12})^T$, no nonlinear terms make any contribution. We have:

$$\text{(A.5)} \qquad b\mathcal{M}_c \left(\begin{array}{c} X_{12} \\ Y_{12} \end{array} \right) = -2ik_c\mathcal{A}_\xi \left(\begin{array}{c} 2 \\ -\frac{1}{2}(1+g) \end{array} \right) \in \text{range}(\mathcal{M}_c).$$

This implies

$$\text{(A.6)} \qquad \left(\begin{array}{c} X_{12} \\ Y_{12} \end{array} \right) = B(\xi,\tau) \left(\begin{array}{c} 2 \\ -\frac{1}{2}(1+g) \end{array} \right) + 2i\frac{k_c}{b}\mathcal{A}_\xi \left(\begin{array}{c} 0 \\ 1 \end{array} \right),$$

where $B(\xi,\tau)$ is a new unknown amplitude term.

The equation for $(X_{13}, Y_{13})^T$ is more complex. The left-hand side is:

$$\text{(A.7)} \qquad b\mathcal{M}_c \left(\begin{array}{c} X_{13} \\ Y_{13} \end{array} \right)$$

The right-hand side has many contributions:

$$\frac{\partial}{\partial t} \left(\begin{array}{c} \delta^{3\beta-2\alpha}U \\ V \end{array} \right) = \mathcal{A}_\tau \left(\begin{array}{c} 2\delta^{3\beta-2\alpha} \\ -\frac{1}{2}(1+g) \end{array} \right) = \mathcal{A}_\tau \left(\begin{array}{c} 0 \\ -\frac{1}{2}(1+g) \end{array} \right) + \text{h.o.t.}$$

$$\text{(A.8)} \qquad \left(\begin{array}{c} U_{xx} \\ V_{xx} \end{array} \right) = \left(\begin{array}{c} 2[\mathcal{A}_{\xi\xi} + 2ik_c B_\xi] \\ -\frac{1}{2}(1+g)[\mathcal{A}_{\xi\xi} + 2ik_c B_\xi] - \frac{4k_c^2}{b}\mathcal{A}_{\xi\xi} \end{array} \right)$$

Writing

$$\text{(A.9)} \quad (X_{02}, Y_{02})^T \equiv |\mathcal{A}|^2 \sqrt{\frac{g}{b}}(x_{02}, y_{02})^T, \qquad (X_{22}, Y_{22})^T \equiv \mathcal{A}^2 \sqrt{gb}(x_{22}, y_{22})^T,$$

we obtain the relevant nonlinear terms:

$$UV \rightarrow \sqrt{\frac{g}{b}}|\mathcal{A}|^2\mathcal{A}[2(y_{02} + y_{22}) - \frac{1}{2}(1 + g)(x_{02} + x_{22})]$$

$$V^2 \rightarrow \sqrt{\frac{b}{g}}|\mathcal{A}|^2\mathcal{A}[-(1 + g)(y_{02} + y_{22})]$$

(A.10) $UV^2 \rightarrow 12g|\mathcal{A}|^2\mathcal{A}$

Define

$$L_{UV} = [2(y_{02} + y_{22}) - \frac{1}{2}(1 + g)(x_{02} + x_{22})]$$

(A.11) $$L_{V^2} = [-(1 + g)(y_{02} + y_{22})]$$

The right-hand side of the equation is then

$$I_1 = 2[\mathcal{A}_{\xi\xi} + 2ik_c B_\xi] - [2gL_{UV} + L_{V^2} + 12g]|\mathcal{A}|^2\mathcal{A} + 4\sqrt{\frac{g}{b}}\mathcal{A}$$

$$I_2 = \frac{1}{2}(1 + g)\mathcal{A}_\tau - \frac{1}{2}(1 + g)[\mathcal{A}_{\xi\xi} + 2ik_c B_\xi] - 2(1 - g)\mathcal{A}_{\xi\xi}$$

(A.12) $$+ [2gL_{UV} + L_{V^2} + 12g]|\mathcal{A}|^2\mathcal{A} - 4\sqrt{\frac{g}{b}}\mathcal{A}$$

To obtain the Ginzburg-Landau equation, we now impose the orthogonality condition (3.25):

(A.13) $(1 + g)\mathcal{A}_\tau - 4(1 - g)\mathcal{A}_{\xi\xi} + \frac{1}{2}(3 - g)L_{tot}|\mathcal{A}|^2\mathcal{A} - 2\sqrt{\frac{g}{b}}(3 - g)\mathcal{A} = 0,$

where $L_{tot} = 2gL_{UV} + L_{V^2} + 12g$. Substituting in for g, we find that

(A.14) $$\mathcal{A}_\tau = \frac{2}{\sqrt{b}}\mathcal{A} + 2\sqrt{2}\mathcal{A}_{\xi\xi} - \frac{1}{2}(\sqrt{2} + 1)L_{tot}|\mathcal{A}|^2\mathcal{A}.$$

Finally, substituting $L_{tot} = \frac{4}{9}(27 - 17\sqrt{2})$ yields equation (3.27).

B. First-order asymptotic correction to A_c. In this appendix, we outline the calculation of the first-order term in the asymptotic expansion of A_c, stated as (6.9) in subsection 6.2. We begin with the formulae (3.7) and (3.9) for k_c^2. By (3.14), we have $2\sigma = 3\beta - 2\alpha$. Also, we will need the first two terms in the asymptotic expansion for the location V_- of the homogeneous steady state (1.2):

(B.1) $$V_-^2 \sim \delta^{2(\alpha-\beta)}\frac{a^2}{b^2} - 2\delta^\alpha a.$$

Hence, (3.7) and (3.9) yield to leading order:

$$k_c^2 = -\delta^{2(\alpha-\beta)}\left[\frac{a_c^2}{2b^2} - \frac{b}{2}\right] + \delta^\alpha\frac{a_c}{2}$$

(B.2) $$k_c^2 = \frac{\delta^{2(\alpha-\beta)}\left[\frac{-2a_c^2}{b} + 6\delta^{2\beta-\alpha}a_c b\right]}{\left(\frac{a_c^2}{b^2} - b\right) - \delta^{2\beta-\alpha}a_c}.$$

Then, binomially expanding the second formula for k_c^2 in (B.2), equating both expressions, multiplying the resulting equation by $2\delta^{-2(\alpha-\beta)}/b$, and rewriting the terms on the right hand side yields, to leading order:

$$(B.3) \qquad -\frac{a_c^2}{b^3} + 1 + \delta^{2\beta-\alpha}\frac{a_c}{b} = \frac{\frac{-4a_c^2}{b^3}}{\frac{a_c^2}{b^3}-1} + 4\delta^{2\beta-\alpha}\frac{\frac{a_c^2}{b}}{\frac{a_c^2}{b^3}-1}\left(\frac{3}{a_c} - \frac{a_c}{a_c^2-b^3}\right).$$

Now, recall that to leading order $a_c^2 = b^3 g$ by Proposition 3.1. Therefore, here we define q via

$$a_c^2 = b^3 g(1 + q\delta^{2\beta-\alpha}) + \mathcal{O}(\delta^{2(2\beta-\alpha)})$$

in order to determine the first order corrections to the result of Proposition 3.1, and we also note that this implies $a_c \sim b^{3/2}\sqrt{g}(1+\delta^{2\beta-\alpha}q/2)$. Now, after first multiplying both sides of (B.3) by $(a_c^2/b^3) - 1$ and then substituting in the expressions for a_c^2 and a_c, we arrive at the same equation (3.16) for the leading order behavior of a_c^2 by equating coefficients on the $\mathcal{O}(1)$ terms, and at the desired equation for q by equating coefficients on all of the $\mathcal{O}(\delta^{2\beta-\alpha})$ terms:

$$-2g^2q + 2gq + \sqrt{g}b(g-1) = -4gq + 4g\sqrt{b}\left(\frac{3}{\sqrt{g}} - \frac{\sqrt{g}}{g-1}\right).$$

Finally, recalling that $g \equiv 3 - 2\sqrt{2}$ and observing that hence $\sqrt{g} = \sqrt{2} - 1$, we get after lengthy algebra:

$$(B.4) \qquad\qquad\qquad q = \sqrt{b}(3 + 2\sqrt{2}).$$

Therefore, we also directly have

$$a_c^2 \sim gb^3\left(1 + \delta^{2\beta-\alpha}\sqrt{b}(3 + 2\sqrt{2})\right)$$

$$(B.5) \qquad a_c \sim \sqrt{g}b^{3/2}\left(1 + \delta^{2\beta-\alpha}\sqrt{b}\left(\frac{3+2\sqrt{2}}{2}\right)\right).$$

Therefore, we have established (6.9) as stated in subsection 6.2.

REFERENCES

[1] J. BILLINGHAM AND D. J. NEEDHAM, *The development of travelling waves in quadratic and cubic autocatalysis with unequal diffusion rates. II. An initial value problem with an immobilized autocatalyst*, Phil. Trans. Roy. Soc. Lond., Series A, 336 (1991), pp. 497–539.

[2] J. G. BLOM AND P. A. ZEGELING, *Algorithm 731: a moving-grid interface for systems of one-dimensional time-dependent partial differential equations*, ACM Transactions in Mathematical Software, 20 (1994), pp. 194–214.

[3] F. H. BUSSE, *Nonlinear properties of thermal convection*, Rep. Prog. Phys., 41 (1978), pp. 1929–1967.

[4] A. DOELMAN, W. ECKHAUS, AND T. J. KAPER, *Slowly modulated two-pulse solutions and the onset of splitting bifurcations in the 1-D Gray-Scott model*, Parts I and II, in press, SIAM J. Appl. Math., 2000.

[5] A. DOELMAN AND P. HOLMES, *Homoclinic explosions and implosions*, Phil. Trans. Roy. Soc. Lond., Series A, 354 (1996), pp. 845–893.

[6] A. DOELMAN, T.J. KAPER, AND P. ZEGELING, *Pattern formation in the one-dimensional Gray-Scott model*, Nonlinearity, 10 (1997), pp. 523–563.

[7] A. DOELMAN, R. A. GARDNER, AND T.J. KAPER, *Stability analysis of singular patterns in the 1-D Gray–Scott model: a matched asymptotics approach*, Physica D, 122 (1998), pp. 1–36.

[8] A. DOELMAN, R. A. GARDNER, AND T. J. KAPER, *A stability index analysis of 1D patterns of the Gray-Scott model*, in press, Memoirs of the AMS, 2000.

[9] W. ECKHAUS, *On modulation equations of the Ginzburg-Landau type*, Proc. Second International Conf. on Indus. and Appl. Math. ICIAM 91, 1992, pp. 83–98.

[10] W. ECKHAUS, *Studies in Nonlinear Stability Theory*, Springer-Verlag, New York, 1965.

[11] J. P. ECKMANN AND C. E. WAYNE, *Propagating fronts and the center manifold theory*, Commun. Math. Phys., 136 (1991), pp. 285–307.

[12] N. FENICHEL, *Geometrical singular perturbation theory for ordinary differential equations*, J. Diff. Eq., 31 (1979), pp. 53–98.

[13] S. FOCANT AND TH. GALLAY, *Existence and stability of propagating fronts of an autocatalytic reaction-diffusion system*, Physica D, 120 (1996), pp. 346–368.

[14] R. A. GARDNER, *On the structure of the spectra of periodic travelling waves*, J. Math. Pures Appl., 72 (1993), pp. 415–439.

[15] R. A. GARDNER, *Spectral analysis of long wavelength periodic waves and applications*, J. reine angew. Math., 491 (1997), pp. 149–181.

[16] P. GRAY AND S. K. SCOTT, *Autocatalytic reactions in the isothermal, continuous stirred tank reactor: isolas and other forms of multistability*, Chem. Eng. Sci., 38 (1983), pp. 29–43.

[17] P. GRAY AND S. K. SCOTT, *Autocatalytic reactions in the isothermal, continuous stirred tank reactor: oscillations and instabilities in the system $A + 2B \rightarrow 3B$, $B \rightarrow C$*, Chem. Eng. Sci., 39 (1984), pp. 1087–1097.

[18] J. K. HALE, L. A. PELETIER, AND W. C. TROY, *Exact homoclinic and heteroclinic solutions of the Gray-Scott model for autocatalysis*, University of Leiden Technical Report Number W98-03, 1998.

[19] G. IOOSS, A. MIELKE, AND Y. DEMAY, *Theory of steady Ginzburg-Landau equation in hydrodynamics stability problems*, Euro. J. Mech. B/Fluids, 8 (1989), pp. 229–268.

[20] G. IOOSS AND M.C. PÉROUÈME, *Perturbed homoclinic solutions in reversible 1:1 resonance vector fields*, J. Diff. Eq., 102 (1993), pp. 62–88.

[21] C. JONES, *Geometric singular perturbation theory*, in Dynamical Systems, Montecatibi Terme 1994, Lecture Notes in Mathematics 1609, Springer, Berlin, 1995.

[22] T. KAPITULA, *On the nonlinear stability of plane waves for the Ginzburg-Landau equation*, Comm. Pure. Appl. Math., 47 (1994), pp. 831–841.

[23] K. J. LEE AND H. L. SWINNEY, *Lamellar structures and self-replicating spots in a reaction-diffusion system*, Phys. Rev. E, 51 (1995), pp. 1899–1915.

[24] K.-J. LIN, W. D. MCCORMICK, J. E. PEARSON, AND H. L. SWINNEY, *Experimental observation of self-replicating spots in a reaction-diffusion system*, Nature, 369 (1994), issue no. 6477, pp. 215–218.

[25] C. MURATOV AND V. OSIPOV, *Spike autosolitons in the Gray-Scott model*, Preprint.

[26] Y. NISHIURA AND D. UEYAMA, *A skeleton structure for self-replication dynamics*, Physica D, 130 (2000), pp. 73–104.

[27] J. E. PEARSON, *Complex patterns in a simple system*, Science, 261 (1993), pp. 189–192.

[28] V. PETROV, S. K. SCOTT, AND K. SHOWALTER, *Excitability, wave reflection, and wave splitting in a cubic autocatalysis reaction-diffusion system*, Phil. Trans. Roy. Soc. Lond., Series A, 347 (1994), pp. 631–642.

[29] W. N. REYNOLDS, J. E. PEARSON, AND S. PONCE-DAWSON, *Dynamics of self-replicating patterns in reaction diffusion systems*, Phys. Rev. Lett., 72 (1994), pp. 2797–2800.

[30] W. N. REYNOLDS, S. PONCE-DAWSON, AND J. E. PEARSON, *Self-replicating spots in reaction-diffusion systems*, Phys. Rev. E, 56 (1997), pp. 185–198.

[31] C. ROBINSON, *Sustained resonance for a nonlinear system with slowly-varying coefficients*, SIAM J. Math. Anal., 14 (1983), pp. 847–860.

[32] V. ROTTSCHÄFER AND A. DOELMAN, *On the transition from the Ginzburg-Landau equation to the extended Fisher-Kolmogorov equation*, Physica D, 118 (1998), pp. 261–292.

[33] G. SCHNEIDER, *Diffusive stability of spatial periodic solutions of the Swift-Hohenberg equation*, Comm. Math. Phys., 178 (1996), pp. 679–702.

[34] G. SCHNEIDER, *Nonlinear diffusive stability of spatially periodic solutions — Abstract theorem and higher space dimensions*, Tohoku Math. Publ., 8 (1998), pp. 159–168.

[35] C. SOTO-TREVINO AND T. J. KAPER, *Higher-order Melnikov theory for adiabatic systems*, J. Math. Phys., 37 (1996), pp. 6220–6249.

[36] J. T. STUART AND R. DIPRIMA, *The Eckhaus and Benjamin-Feir resonance mechanisms*, Proc. Roy. Soc. Lond. A, 362 (1978), pp. 27–41.

[37] A. M. TURING, *The chemical basis of morphogenesis*, Phil. Trans. Roy. Soc. Lond., Series B, 237 (1952), pp. 37–72.

[38] P. A. ZEGELING, J. G. VERWER, AND J. C. H V. EIJKEREN, *Application of a moving-grid method to a class of 1D brine transport problems in Porous media*, International Journal for Numerical Methods in Fluids, 15 (1992), pp. 175–191.